Session 4/ 12.30h – 13.00h:
Flow Dynamics

RES Engineering Seminar 15th October, 2014

MIXING FEATURES OF SWIRLING FLOWS IN COMBUSTORS

Researchers:

Teresa Parra-Santos — *Dept. Energy Engineering & Fluid Mechanics*
Ruben Perez-Dominguez — *University of Valladolid (Spain)*
Victor M. Mendoza-García

Supervisors:

Robert Z. Szasz — *Energy Division, Lund University (Sweden)*
Ville Vuorinen — *Dept. of Energy Technology, University of Aalto (Finland)*

ESCUELA de INGENIERÍAS INDUSTRIALES

GOBIERNO DE ESPAÑA MINISTERIO DE CIENCIA E INNOVACIÓN

PRACE

OVERVIEW

- Numerical Model
- Validation
- Influence of Swirl number
- Influence of Diffuser
- Influence of Stoichiometry

Two approaches:

- Isothermal Cases using LES
- Mixing and Reactive Cases using Swirl dominated RNG *k*-ε

Aim and Justification

- To achieve lean flame stability and ultralow emissions.
- Actual trends:
  - Bluff body
  - Cross flows

  } ↑ ΔP, ↑T, soot

  - Swirl burner ↓T, ↓ ΔP, lean flames

$$S = \frac{\int \rho (r v_\theta) v_z 2\pi r dr}{R \int \rho v_z^2 2\pi r dr}$$

- Flow Pattern
  - Low-swirl burner (S < 0.5)
    - Central Divergence Zone
    - Shear Layer
    - Outer Recirculation Zone
  - High-swirl burner (S > 0.5)
    - Inner Recirculation Zone
    - Shear Layer
    - Outer Recirculation Zone

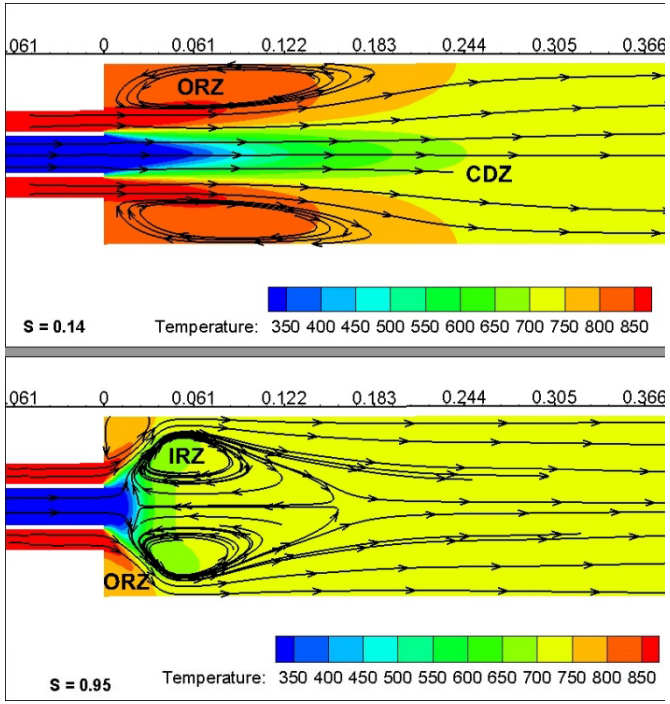

Benchmark: Test case of Roback & Johnson

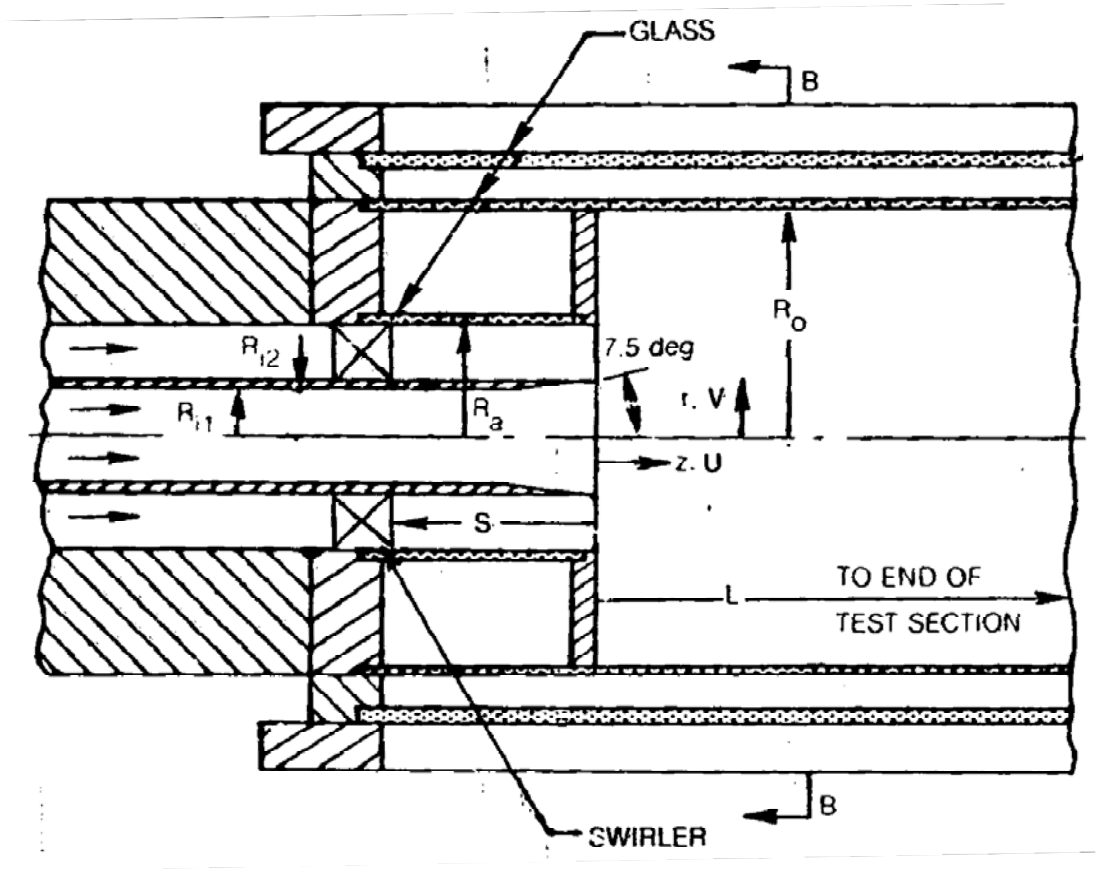

Isothermal (no combustion)

Ref. Roback R., Johnson B.V. (1983) Mass and momentum turbulent transport experiments with confined swirling coaxial jets, NASA CR-168252

	Roback & Johnson	Re
R_{i1}	12.5 mm	3617
R_{i2}	15.3 mm	
R_a	29.5 mm	1129
R_o	61.0 mm	2973
S	50 mm	
L	1 m	
ER (R_o/R_a)	2.0678	
Q_{an}/Q_{cn}	9.377	
V_{an}	1.52 m/s	
V_{cn}	0.66 m/s	
V_{an}/V_f	5.2855	
V_{cn}/V_f	2.295	

Physical model: Swirl number 1.2

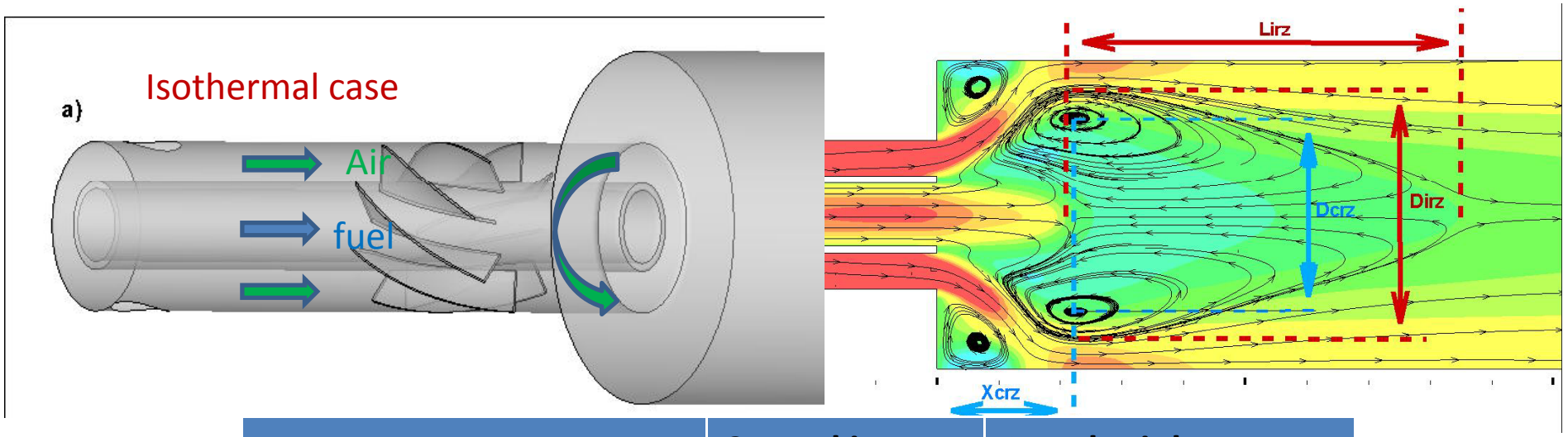

	Central jet	Annular inlet
Velocity	0.66 m/s	1.54 m/s
Diameter	0.025 m	0.028 m
Density	1.225 kg/m^3	
Viscosity	1.7894 10^5 kg/(ms)	
Intensity of turbulence	12%	7.5%
k	0.00310 m^2/s^2	0.06600 m^2/s^2
$\varepsilon = c_\mu^{0.75} k^{1.5} / \ell$	0.00567 m^2/s^3	0.6925 m^2/s^3

- S = 1 generated with eight-flat-vane swirler of 62º pitch angle and 25 mm chord => Forced vortex

Challenges working with HPC

- Parallel processing using OpenFoam.
  - Optimum method of spatial decomposition.
  - Minimize the number of interface cells: scotch.

- LES
  - Uniform hexahedral Mesh
  - Enough spatial and time resolution if energy spectrum is correctly predicted.
  - Different postprocess tasks
    - Special treatment of the data: time averaged fields, Labda2, …
    - Analysis of frequency domain that request frequent snapshots, register of probes located on free turbulence zones.

Time averaged and instantaneous flow

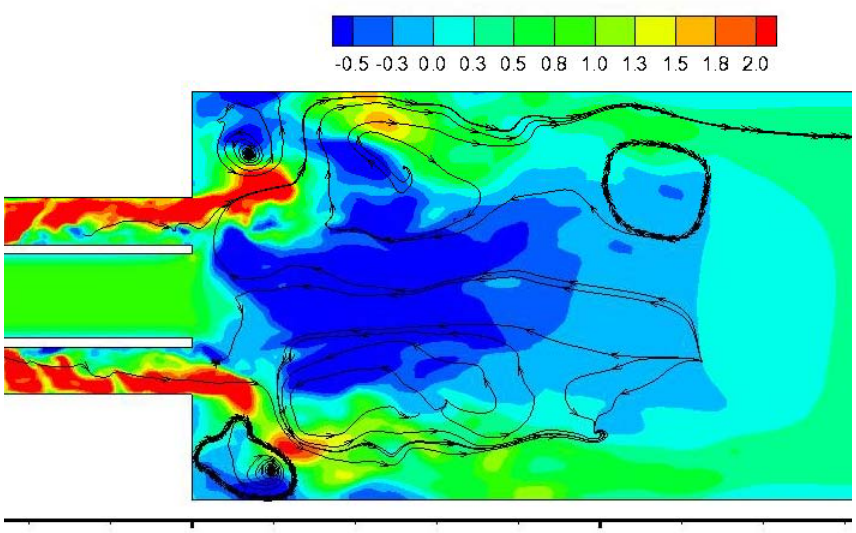

Instantaneous flow

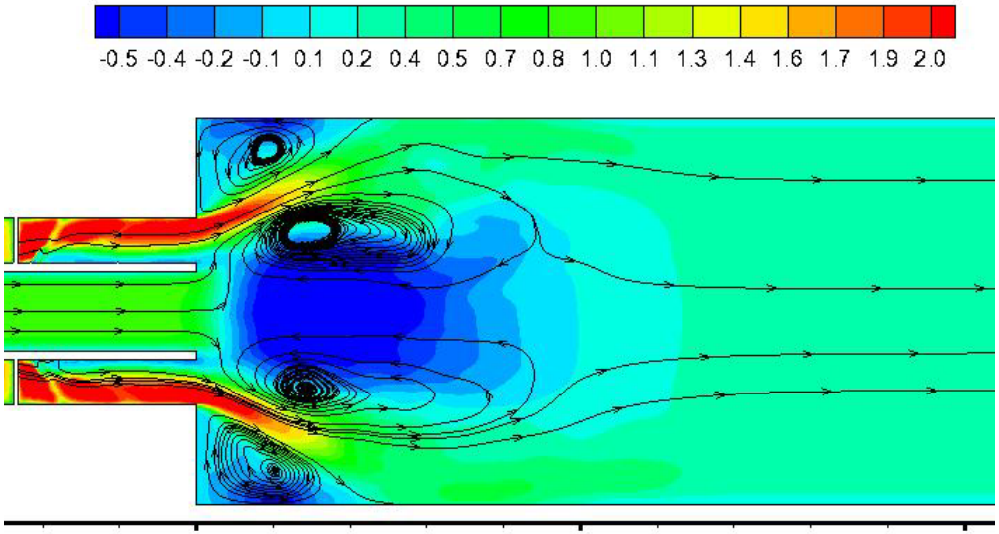

Mean flow

- It is hard to predict flow patterns from instantaneous fields.
  - backflow with negative averaged velocities are often positive in instantaneous fields.
  - Streamlines can be far from being comprehensible
- Only after full convergence has been achieved, the time average can start.

LES Requisites

- LES treatment models small isotropic turbulent scales. Hence a Driest's wall-damping function is necessary to cancel sub-grid stress viscosity near walls

$$f_\mu = 1 - \exp\left(-\frac{y^+}{25}\right)$$

$$\mu_{sgs} = f_\mu \rho (C_s \Delta)^2 \sqrt{2\bar{S}_{ij}\,\bar{S}_{ij}}$$

- Besides, it requires very fine mesh in all directions near walls, not only in the near-wall direction. [Davidson, 2007] proposed spatial resolution on the wall.

$$\Delta y^+ = 1,\ \Delta x^+ = 100,\ \Delta z^+ = 30$$

Implicit LES Model

- Implicit LES (ILES) can be applied in numerical simulations of transitional flows.
- Filter width Δ is related to the mesh size Δ_i , then no subgrid model is applied.
- Since the subgrid stress tensor has a dissipative nature, this role is played by the numerical error such as proposed by Boris and Oran among others [Bensow, 2010].
- The numerical error is controlled using different kind of limiters and schemes,

```
div(phi,U)    Gauss limitedLinearV 0.005;
```

  TVD scheme with a coefficient looking for good accuracy.
- $\Delta y^+ = 1$ is a prerequisite.

Refined Models

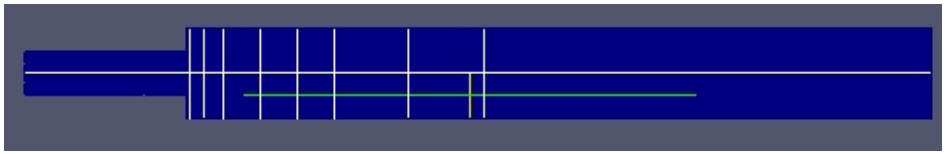

- Spatial resolution 2.5 million cells:
  - annular nozzle Δ~d/22;
  - central nozzle Δ~d/32;
  - test chamber Δ~d/110.
- Wall y+: $\Delta y_{min}^{+} = 0.3255$, $\Delta y_{av}^{+} = 6.195$

- Spatial resolution 10 million cells:
  - annular nozzle Δ~d/46;
  - central nozzle Δ~d/40;
  - test chamber Δ~d/110.
- Wall y+: $\Delta y_{min}^{+} = 0.049$, $\Delta y_{av}^{+} = 2.53$

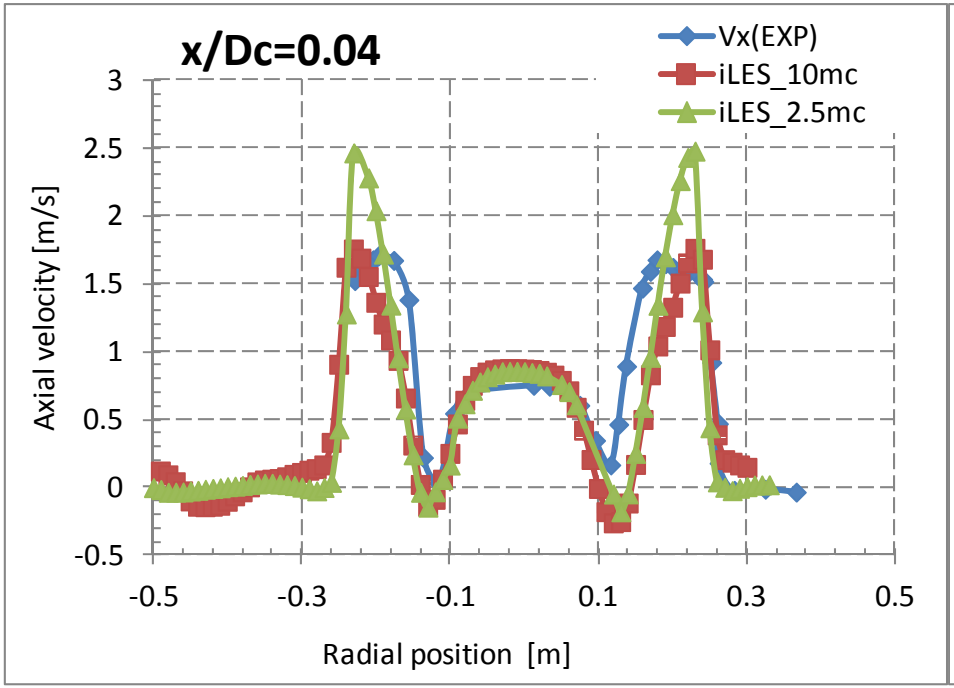

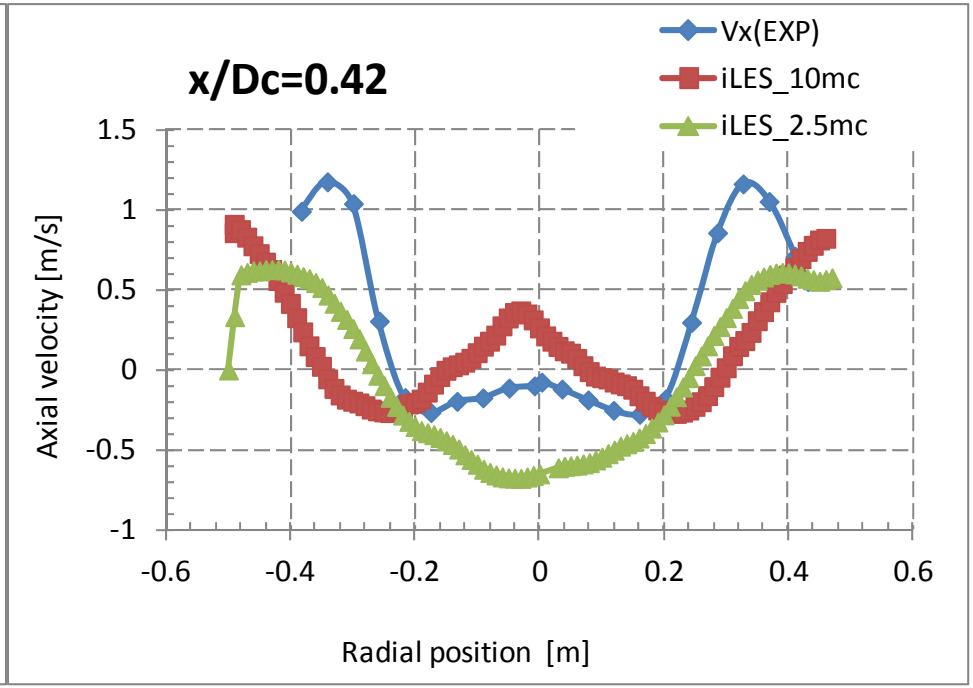

ILES Results

x/D = 0.83

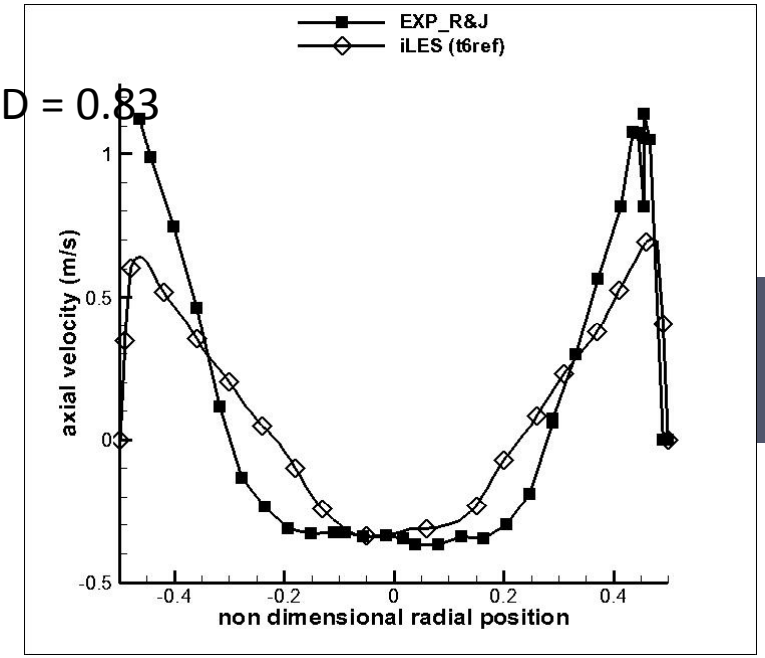

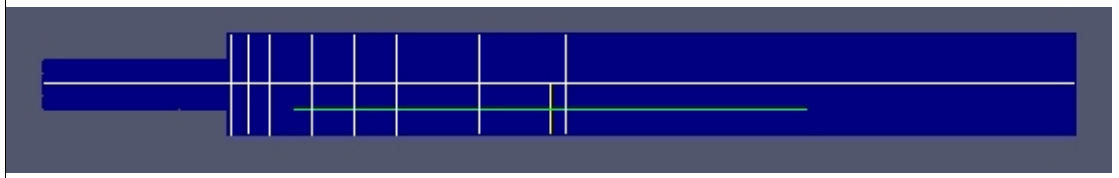

x/D = 1.25

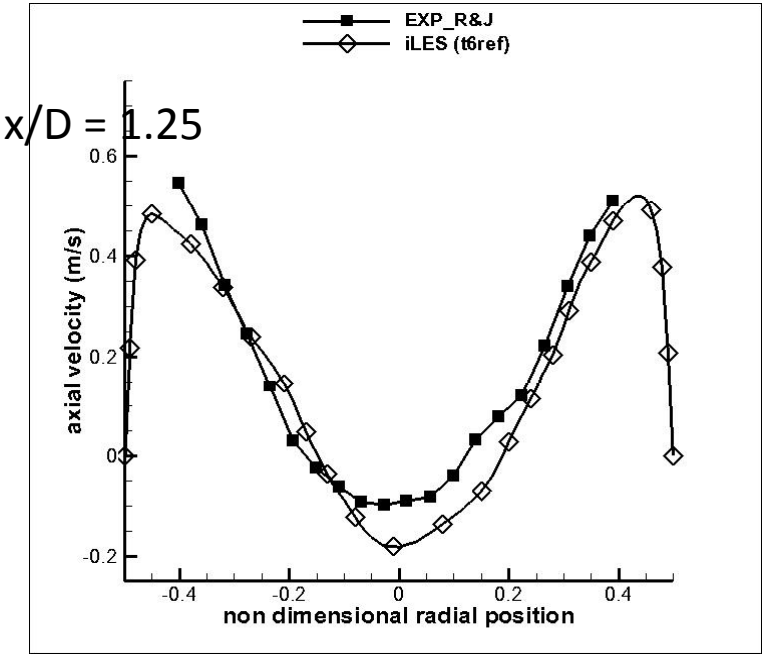

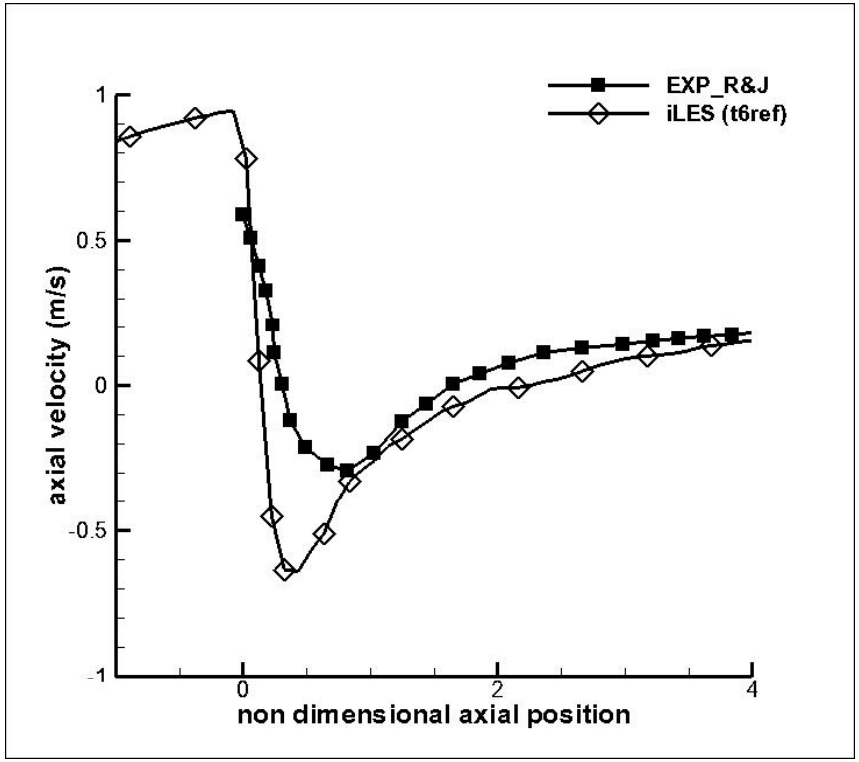

ILES Results

UMean	
U	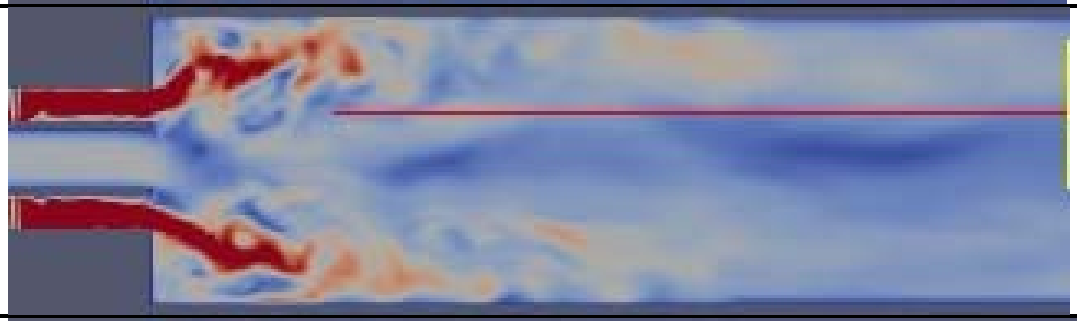
Uprime2Mean<0.5	

ILES Results

Ps

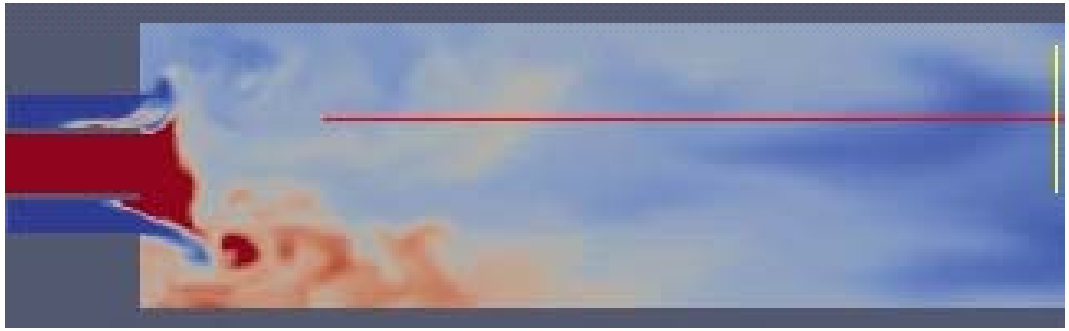

Sigmaxx <0.005

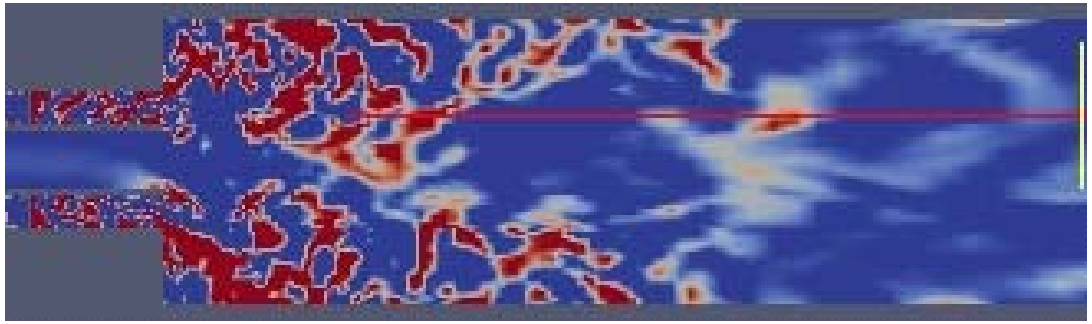

Scale Selective Discretization

- This method is proposed by [Vourinen, 2012]
- Separation of the scales is performed using a high-pass filter. For non uniform meshes, the laplacian filter has the expression:

$$u'_i = -\frac{\partial}{\partial x_j}\left(\frac{\Delta_i}{\pi}\right)^2 \frac{\partial u_i}{\partial x_j}$$

  filter operator is identified as the Nyquist wavenumber to the power of -2.
- Decomposition the velocity field into the smooth and the fluctuating parts.

$$div(\vec{u}u_i) = \frac{\partial}{\partial x_j}\left[u_j\left(u_i - u'_i + u'_i\right)\right] = \frac{\partial}{\partial x_j}\left[u_j\left(u_i - u'_i\right)\right] + \frac{\partial}{\partial x_j}\left(u_j u'_i\right)$$

  The first one is solved with a second order scheme whereas the second is solved with a blended scheme between first and second order.

Implicit LES Model with Scale Selective Discretization

- In case of an implicit resolution, the non-linear term is not transformed and two source terms are added on the RHS of the momentum equation as forces.

$$f_{m,i} = -\frac{\partial}{\partial x_j}\left[u_j u'_{1i}\right] + \frac{\partial}{\partial x_j}\left(u_j u'_{2i}\right)$$

Where the fields u'_{1i} and u'_{2i} are equal and result from the same Laplacian filter. Once again each term must be solved with different schemes.

Validation

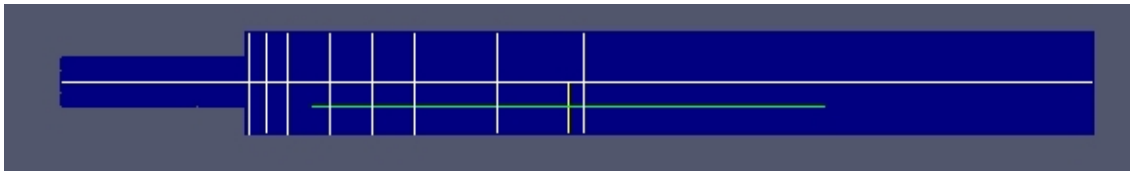

Wall y+ $\Delta y_{min}^{+} = 0.291$, $\Delta y_{av}^{+} = 6.447$

	Axial Velocity	Radial Velocity	Azimuthal Velocity
Axial length 100 mm	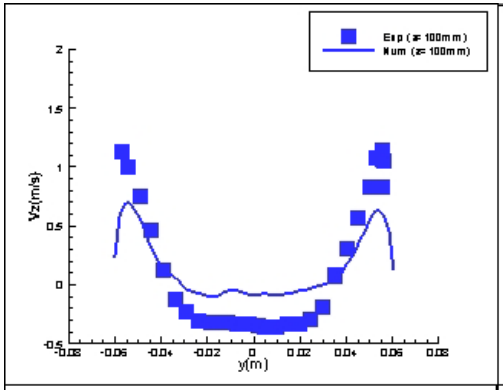	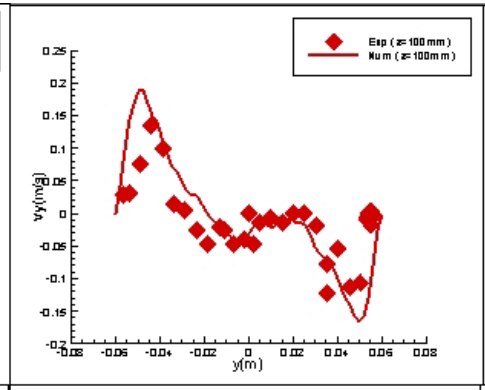	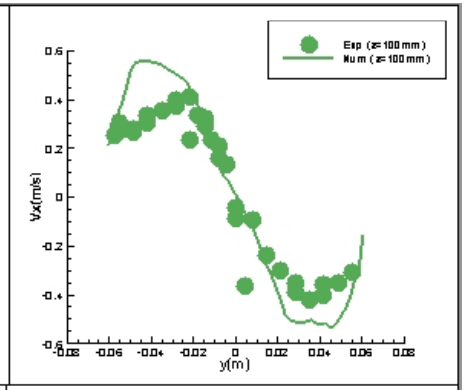
Axial length 160 mm	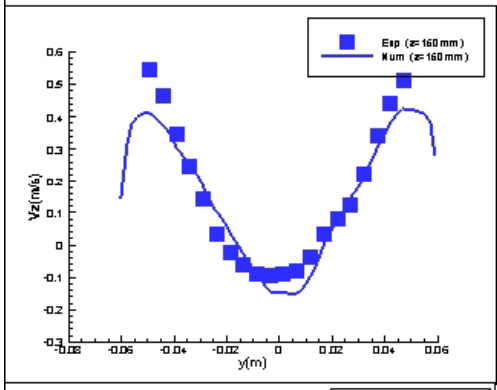	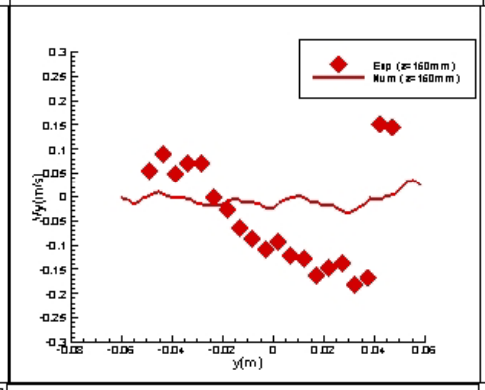	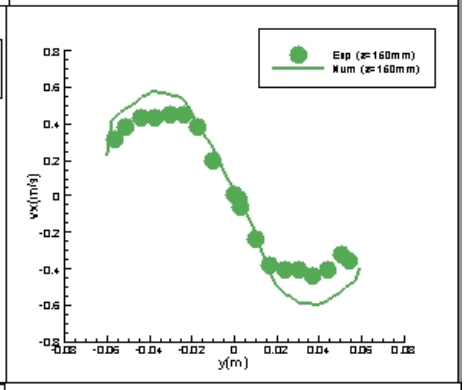
Axial length 200 mm	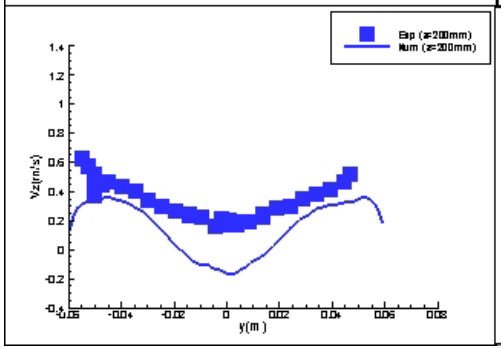	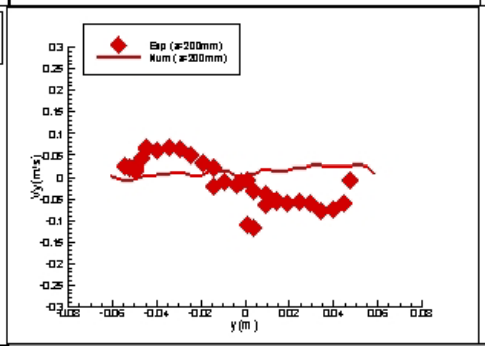	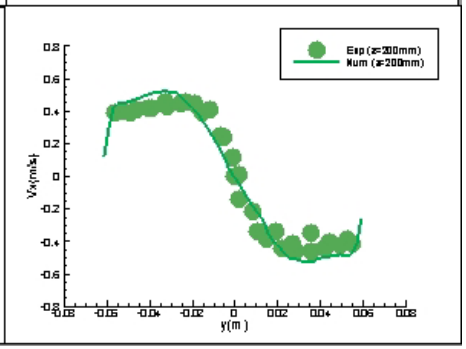

ILES-SSD Results

UMean

U

Uprime2Mean<0.5

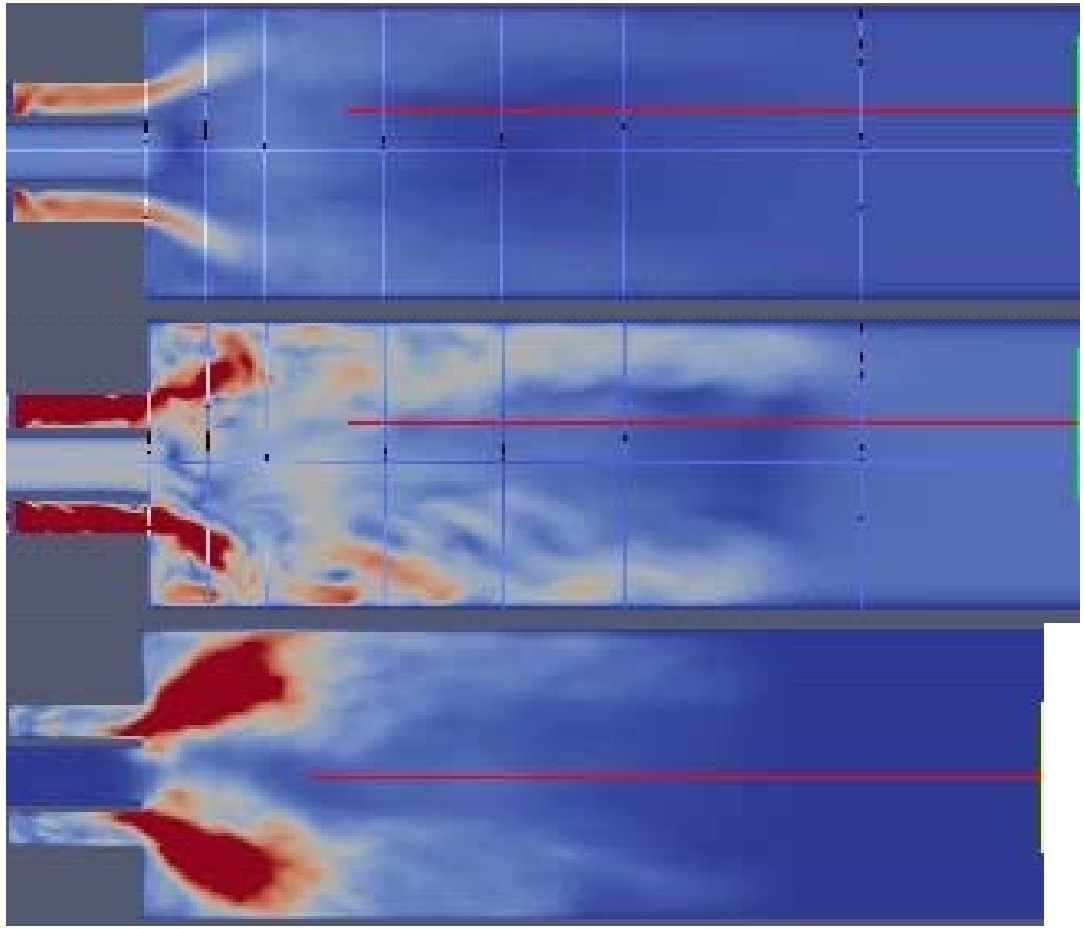

ILES-SSD Results

Ps < 0.1

Lambda2 $\in$(-1000,1000)

rhoUprime <0.05

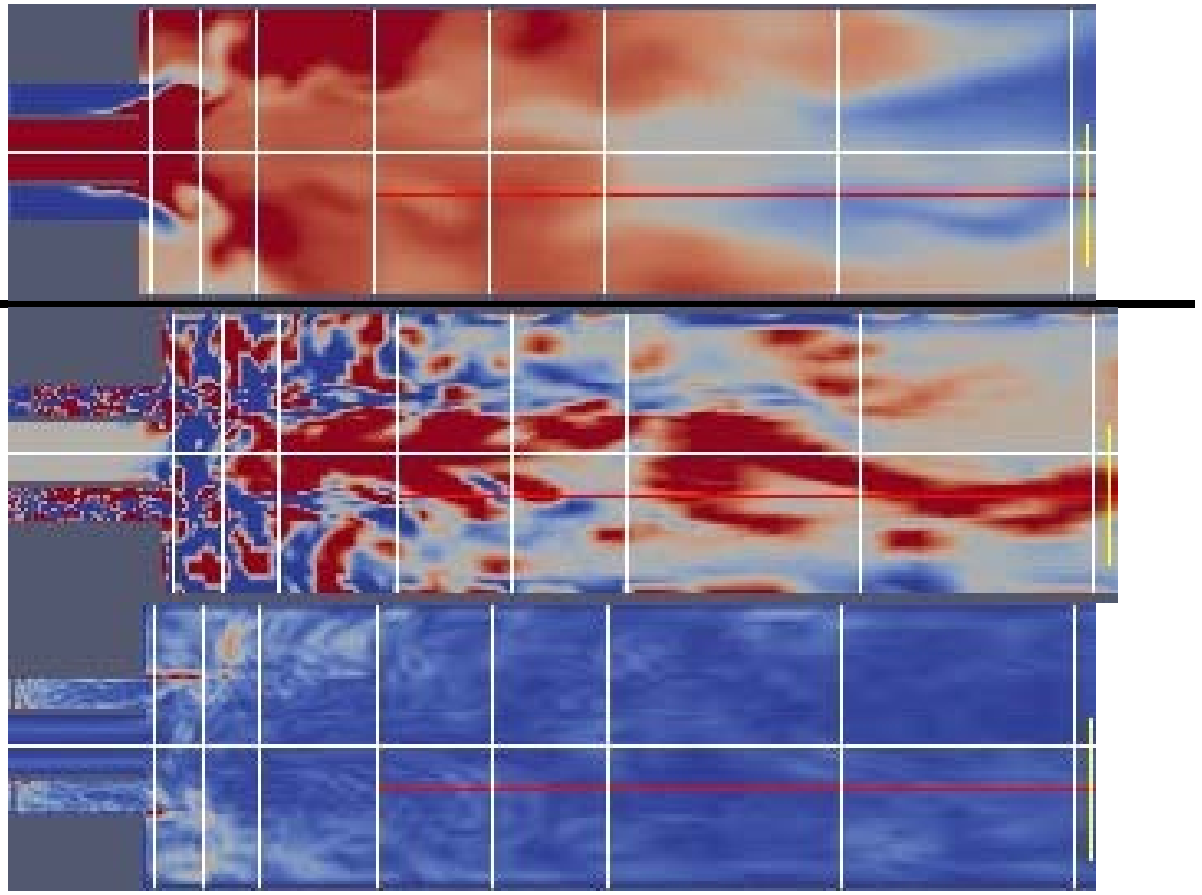

Criterion λ_2 for vortex identification

- Contours of vorticity components or the pressure field made difficult to identify local low-pressure areas.
- Where λ_2 is the intermediate eigenvalue of the tensor $S^2+\Omega^2$
- $\lambda_2 < 0$ represents locations in the flow where the rotation dominates shear.

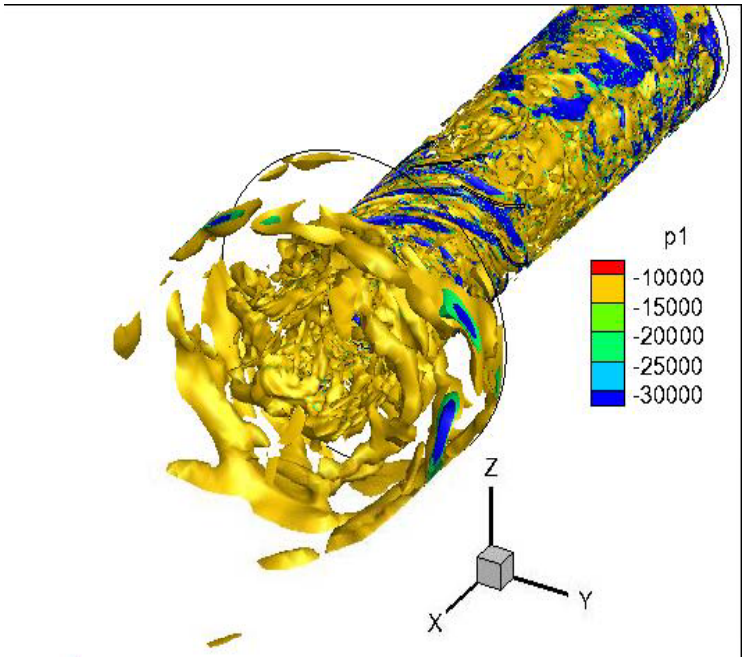

Criterion Q for vortex identification

- Q defined as: $$Q = -\frac{1}{2}\left(S_{ij}S_{ij} - \Omega_{ij}\Omega_{ij}\right).$$

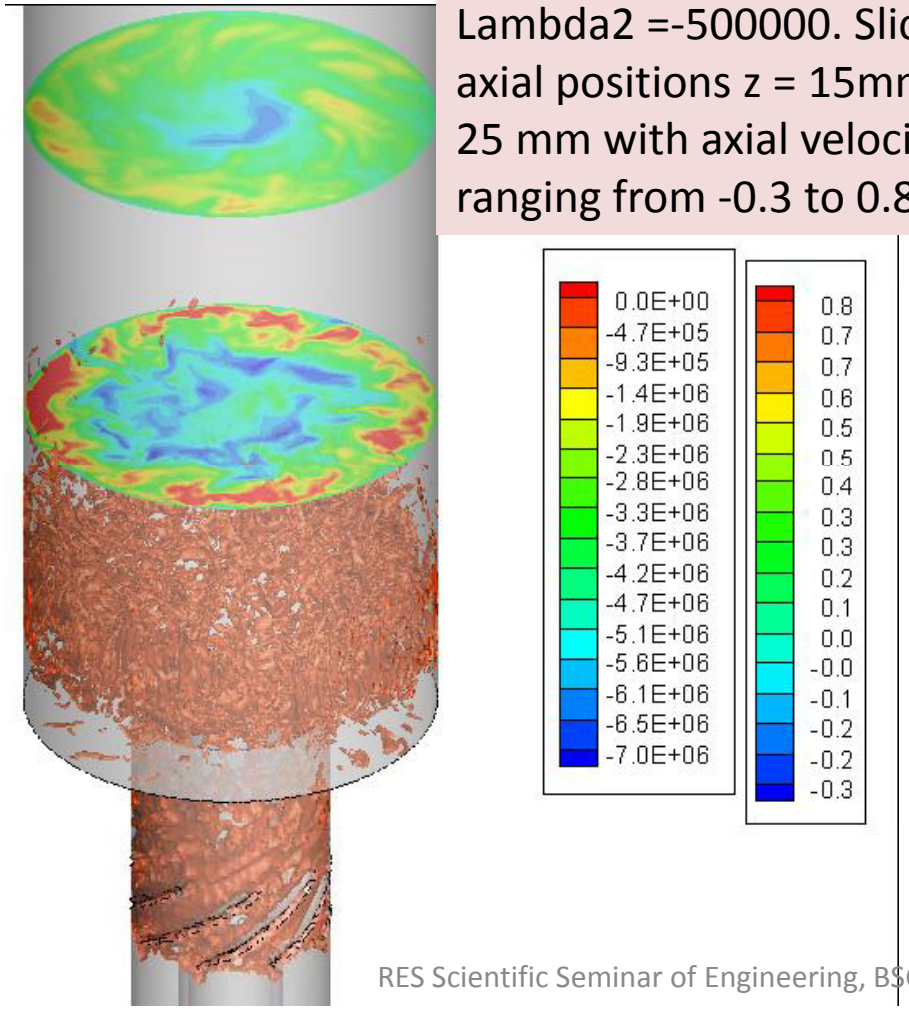

Lambda2 =-500000. Slices at axial positions z = 15mm and 25 mm with axial velocity ranging from -0.3 to 0.8 ms^{-1}.

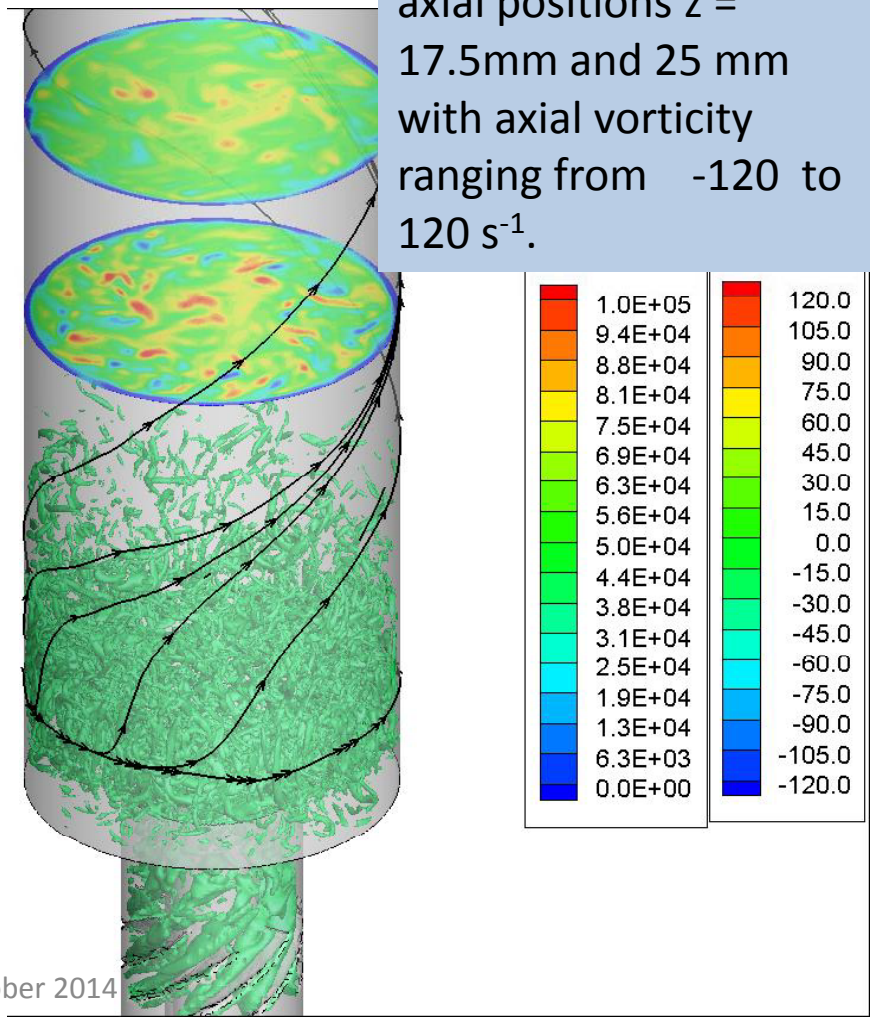

Q =30000. Slices at axial positions z = 17.5mm and 25 mm with axial vorticity ranging from -120 to 120 s^{-1}.

- The full spectrum is given by:

$$E(\kappa) = f_L f_\eta 1.5\, \varepsilon^{2/3}\, \kappa^{-5/3}$$

Taylor's hypothesis of frozen turbulence.

- Determination of the spectrum requires simultaneous measurements of all velocity components at multiple points.
- It is common to measure one velocity component at one point over a certain period of time and convert the time signal to a spatial signal using x = Ut with U being the time averaged velocity. It is only valid for u'/U << 1, which is not always the case.

Energy decay for Re_L=2400

- Taylor-scale Reynolds number R_λ is related to the turbulence Reynolds number as :

$$Re_\lambda = \left(\frac{20}{3} Re_L \right)^{1/2}$$

$$Re_L = \frac{k^2}{\varepsilon \nu}$$

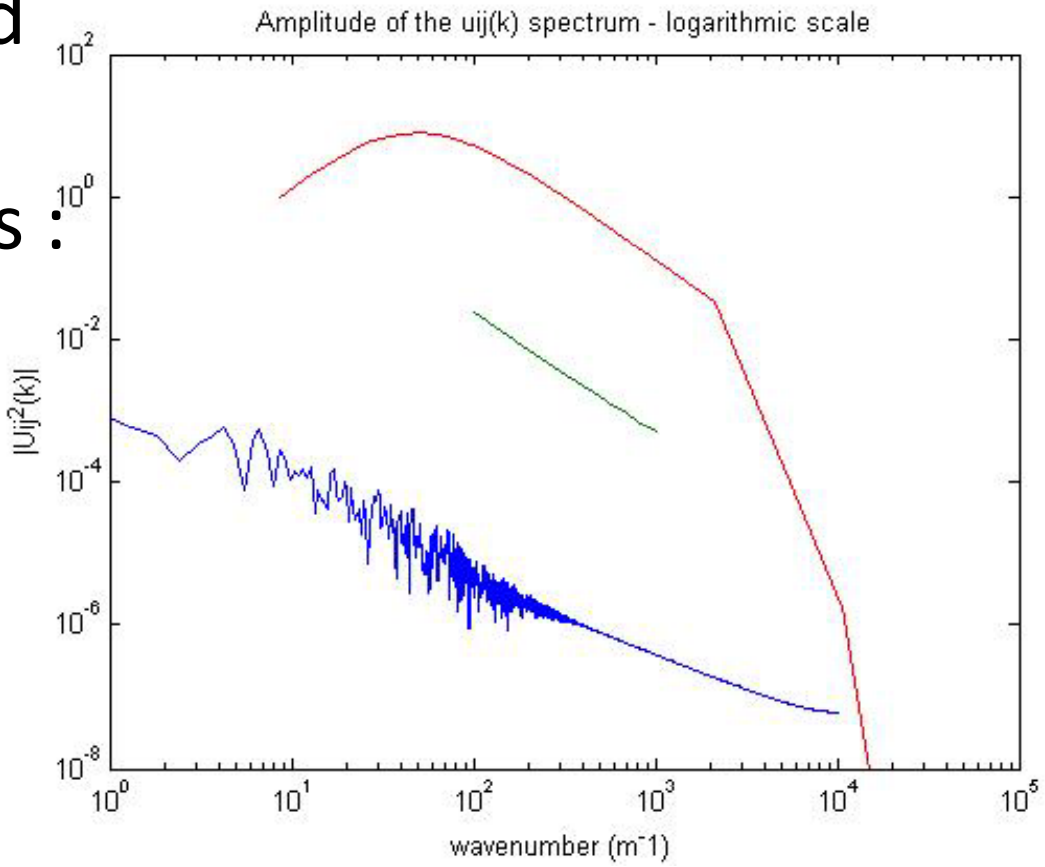

- In the case of R&J

$$Re_L = 2400 \Rightarrow Re_\lambda = 126$$

$$\eta = 0.17 \text{ mm}$$

POD recipe

- Arrange fluctuating part of velocity components for the N snapshots as:

$$\mathbf{U} = [\mathbf{u}^1 \ \mathbf{u}^2 \ \dots \ \mathbf{u}^N] = \begin{bmatrix} u_1^1 & u_1^2 & \dots & u_1^N \\ \vdots & \vdots & \vdots & \vdots \\ u_{lm}^1 & u_{lm}^2 & \dots & u_{lm}^N \\ v_1^1 & v_1^2 & \dots & v_1^N \\ \vdots & \vdots & \vdots & \vdots \\ v_{lm}^1 & v_{lm}^2 & \dots & v_{lm}^N \end{bmatrix}$$

- Calculate Covariance matrix:

$$\tilde{\mathbf{C}} = \mathbf{U}^T\mathbf{U}$$

- Solve the eigenvalues:

$$\tilde{\mathbf{C}}\mathbf{A}^i = \lambda^i \mathbf{A}^i$$

- Order the eigenvalues:

$$\lambda_1 > \lambda_2 > \dots > \lambda_N = 0$$

- POD modes are:

$$\boldsymbol{\phi}^i = \frac{\sum_{n=1}^{N} A_n^i \mathbf{u}^n}{\left\| \sum_{n=1}^{N} A_n^i \mathbf{u}^n \right\|}, \qquad i = 1, \dots, N$$

POD at x = 50mm, 400 samples $\Delta t = 10^{-4}$ s

Energy of each modes

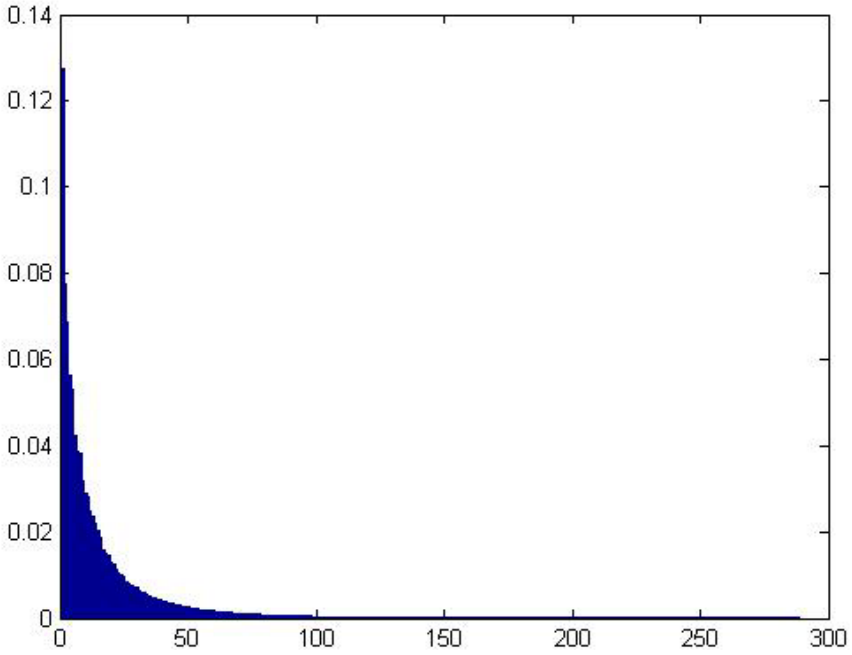

Mode 0: Averaged Flow

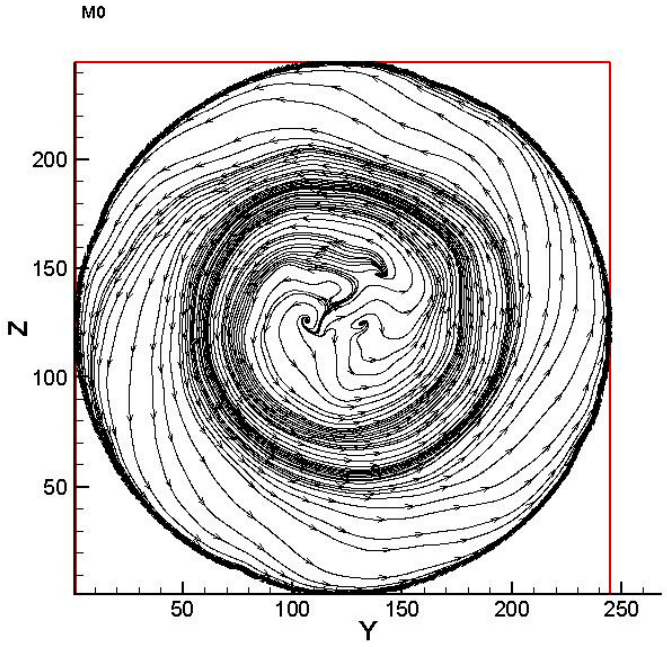

POD at x = 50mm

Modes 1-2

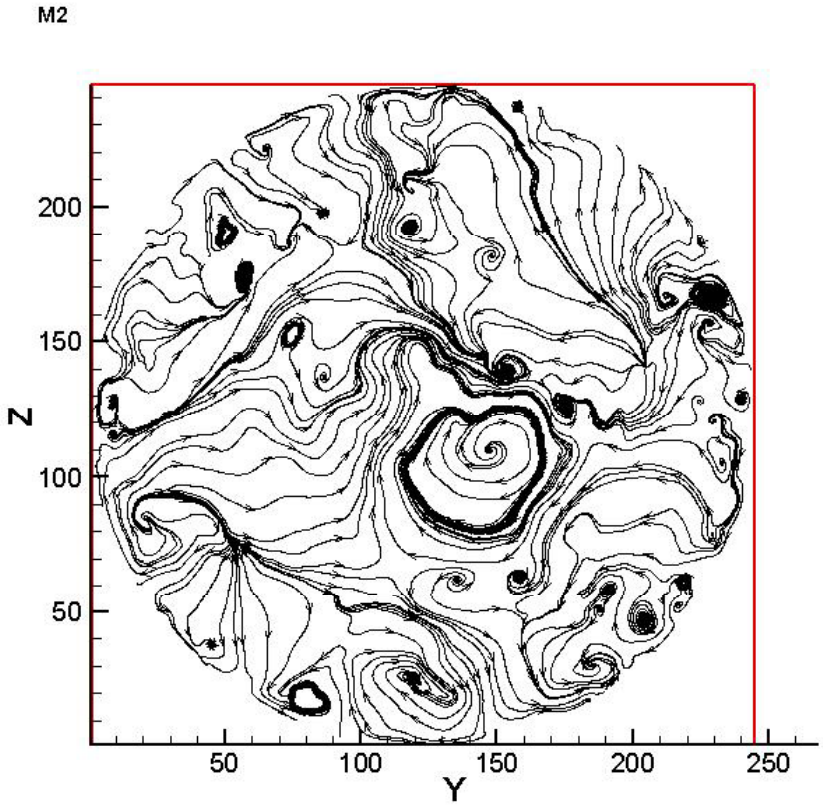

Modes 3-4

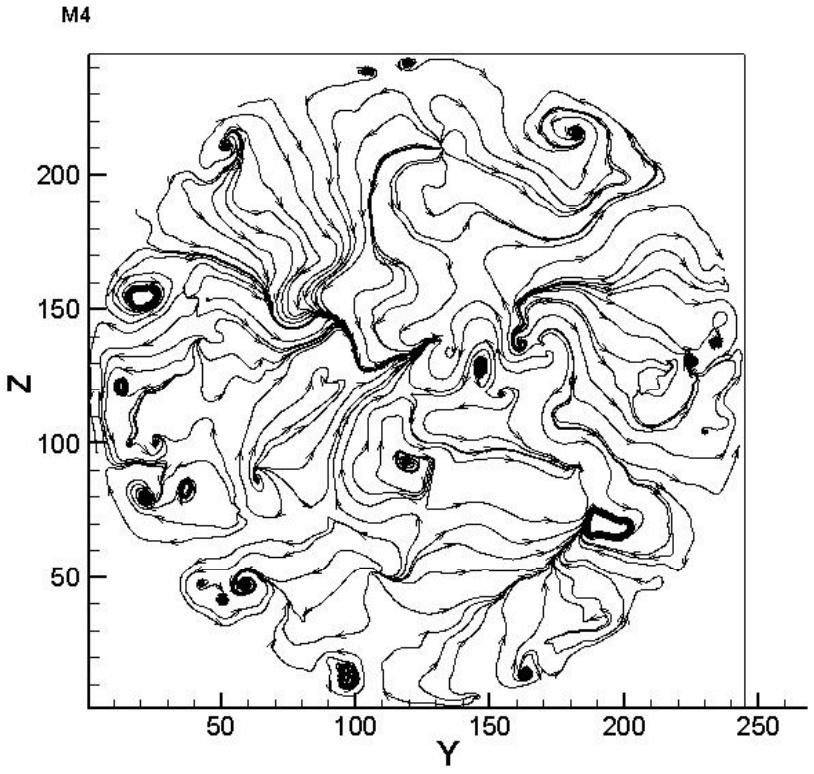

Precessing Vortex Core (PVC)

- The centre of instantaneous IRZ is not located in the axis of the chamber. The temporal sampling of instantanous azimuthal velocities evidences this centre spins around the axis.
- The frequency of spinning corresponds with a Strouhal number around 2.83 calculated based on the chamber diameter and its bulk velocity.

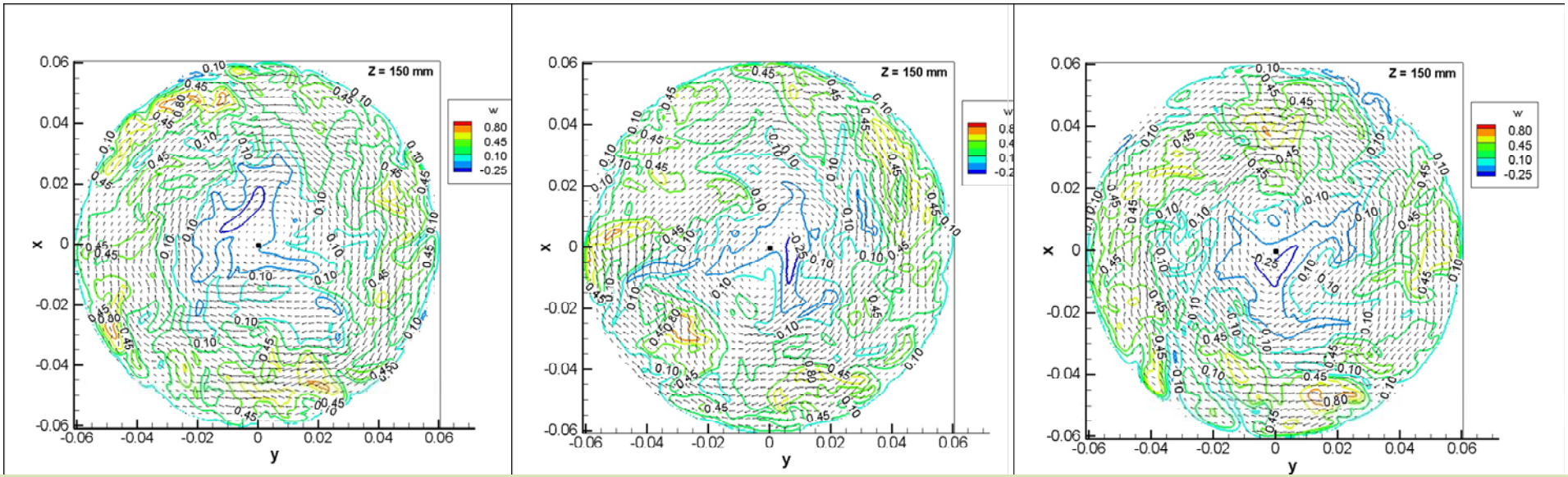

Instantaneous velocity field in the transversal section Z = 0.15 m. Contours correspond with tangential velocity over velocity vectors.

Parametric Study

Swirl number is produced by 8 flat blades of different angles

Swirl	0.6	1	1.2
Trailing Edge Angle	45º	62º	75º
Chord (m)	0.05	0.05	0.05

Model	NoDif	Dif_160	Dif_140	Dif_120	Dif_90	Dif_60
Diffuser angle	180º	160º	140º	120º	90º	60º

Different conical diffusers

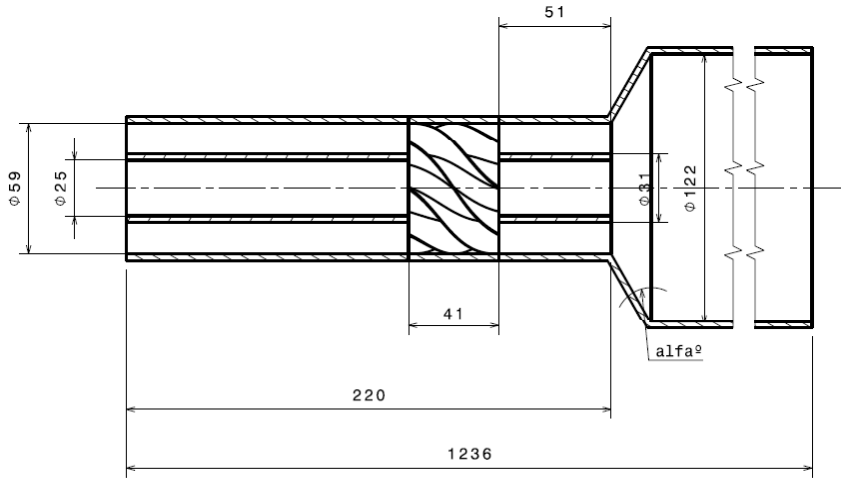

Influence of Swirl & Diffuser

- No_Dif and diffuser 60º
- Contours of Averaged Axial Velocity

S=1.2

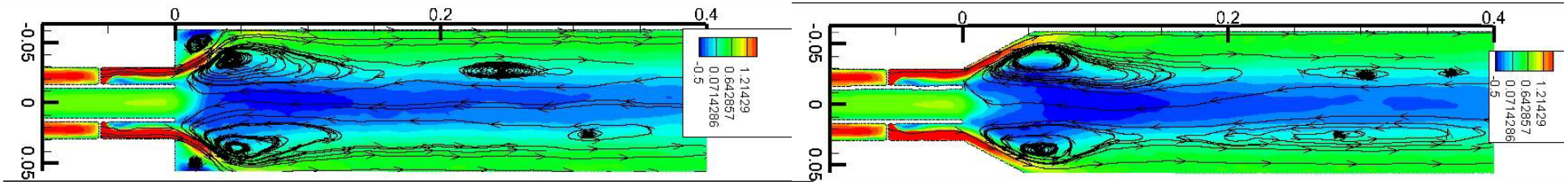

S=0.6

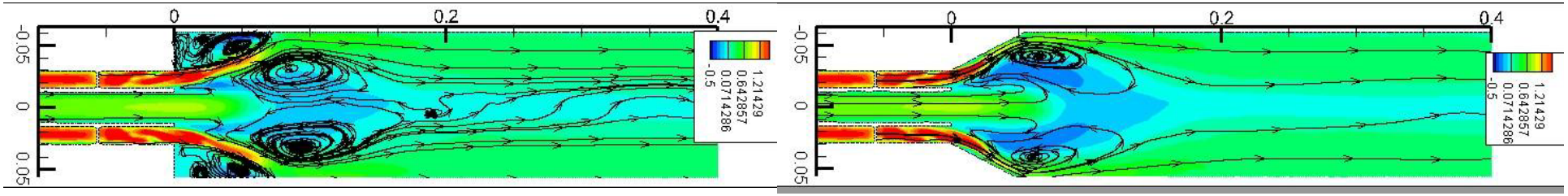

S =1.2 Averaged Axial Velocity

- Diffusers 60º, 90º, 120º, 140º, 160º and No_Dif

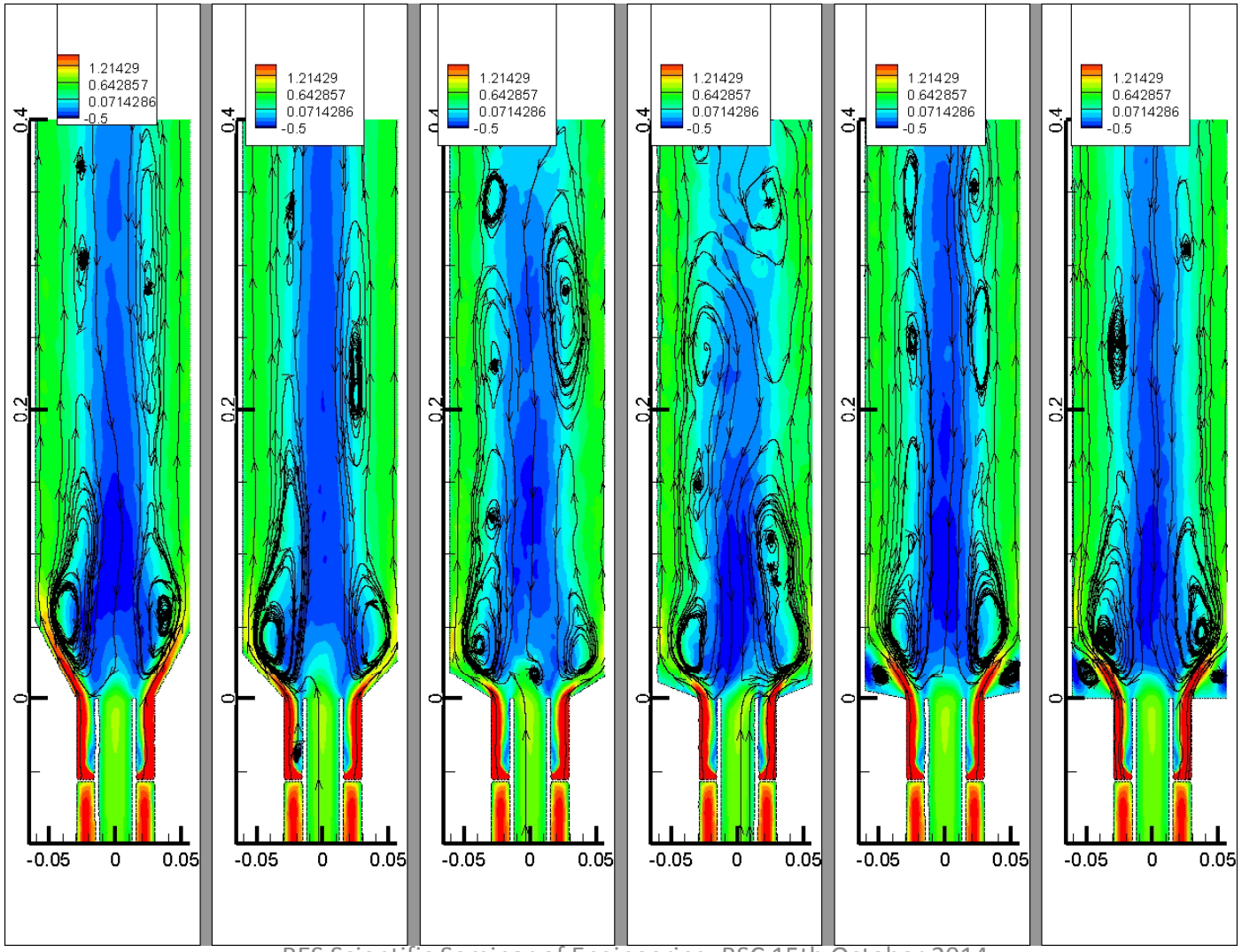

S =0.6 Averaged Axial Velocity

- Diffusers 60º, 90º, 120º, 140º, 160º and No_Dif

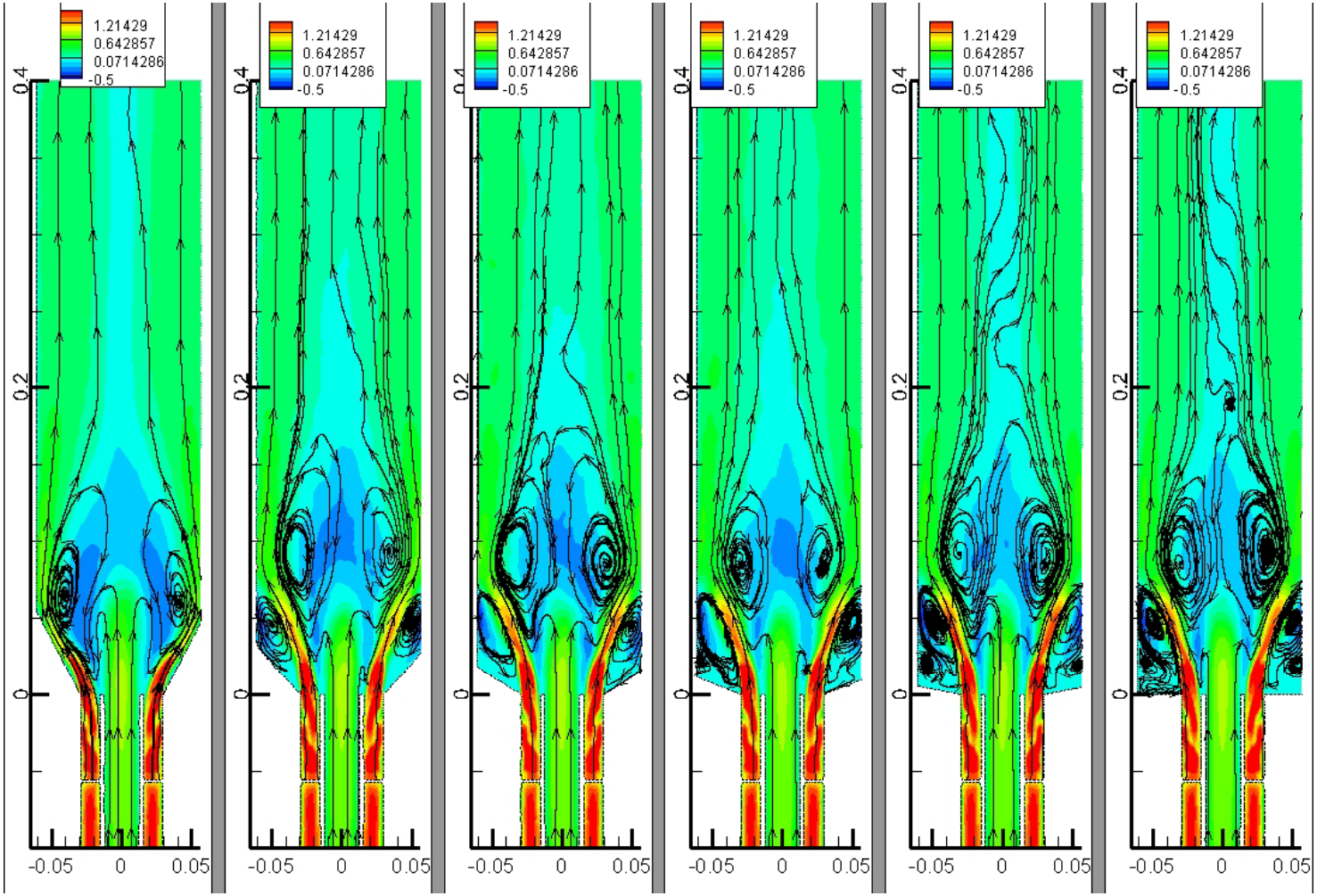

Passive Scalar

- Diffusers 60º, 90º, 120º, 140º, 160º and No_Dif

S =1.2

S =0.6

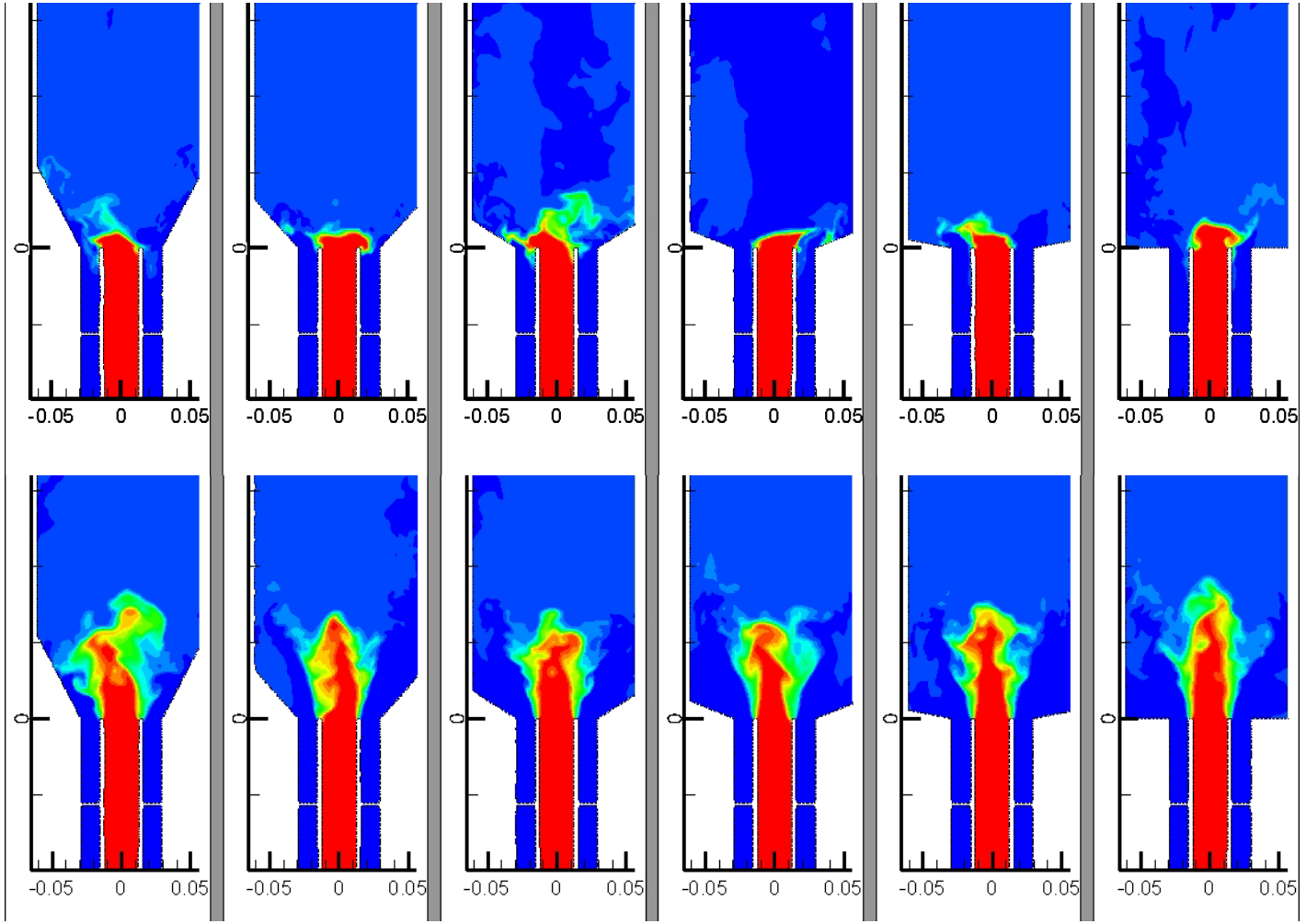

Conclusions of LES Isothermal Cases

- iLES and SSD+iLES are very challenging approach to model flows.
- Averaged fluid field was validated with experimental results provided by Roback and Johnson.
- The analysis on the frequency domain let identify energetic vortex structures using Proper Orthogonal Decomposition.
- Strong swirl numbers produce larger IRZ and smaller ORZ than low swirl numbers.
- Diffuser prevents or reduces the ORZ

Numerical Model of Multi-Species

- Geometrical model of [Roback, 1983]
- Swirl generator: 8 fixed blades. Different swirl numbers

Swirl	0.14	0.74	0.95
Trailing Angle	25º	54º	64º

- Mesh of 5 M grid points
- Second order upwind

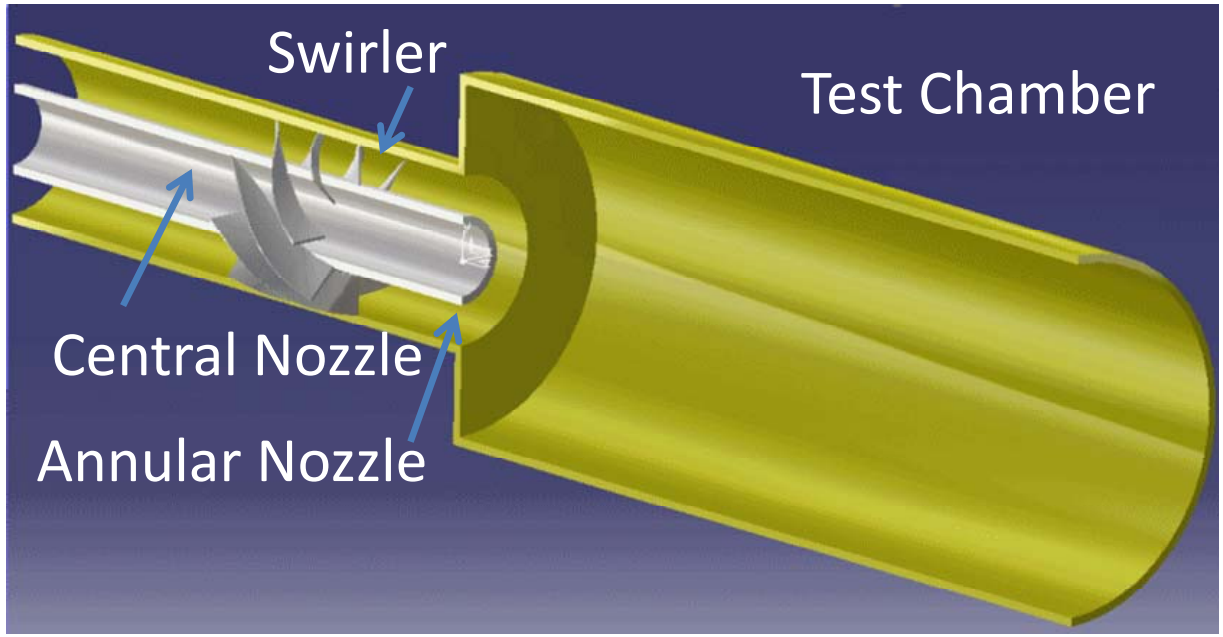

	Central Nozzle	Annular Nozzle
Axial Velocity (m/s)	0.66	1.52
Turbulence Intensity (%)	7.5	12
Hydraulic diameter	0.025	0.03
Temperature (K)	300	900
Mass fraction	90%CH_4 +10% N_2	22%O_2 + 78%N_2

	Roback & Johnson
R_{i1}	12.5 mm
R_{i2}	15.3 mm
R_a	29.5 mm
R_o	61.0 mm
S	50 mm
L	1 m

RNG *k*-ε

- Swirl dominated RNG *k*-ε is suitable for non isotropic flows

$$\frac{\partial}{\partial t}(\rho k) + \frac{\partial}{\partial x_i}(\rho k u_i) = \frac{\partial}{\partial x_j}\left(\alpha_k \mu_{eff} \frac{\partial k}{\partial x_j}\right) + G_k - \rho\varepsilon$$

$$\frac{\partial}{\partial t}(\rho \varepsilon) + \frac{\partial}{\partial x_i}(\rho \varepsilon u_i) = \frac{\partial}{\partial x_j}\left(\alpha_\varepsilon \mu_{eff} \frac{\partial \varepsilon}{\partial x_j}\right) + C_{1\varepsilon}\frac{\varepsilon}{k} G_k - C_{2\varepsilon}\rho\frac{\varepsilon^2}{k} - R_\varepsilon$$

C_μ	$C_{1\varepsilon}$	$C_{2\varepsilon}$	η_0	β
0.0845	1.42	1.68	4.38	0.012

- The term R_ε represents the rate of strain defined by

$$R_\varepsilon = \frac{C_\mu \eta^3 \rho (1 - \eta/\eta_0)}{1 + \beta\eta^3}\frac{\varepsilon^2}{k}$$

$$\eta = \left(2 S_{ij} S_{ij}\right)^{0.5} k/\varepsilon$$

Combustion Model: *Probability Density Function*

- Mean Mixture Fraction equation

$$\frac{\partial}{\partial t}(\rho\bar{f}) + \frac{\partial}{\partial x_i}(\rho u_i \bar{f}) = \frac{\partial}{\partial x_i}\left(\frac{\mu_t}{\sigma_t}\frac{\partial}{\partial x_i}\bar{f}\right)$$

σ_t	C_g	C_d
0.7	2.86	2

- Mixture Fraction Variance equation

$$\frac{\partial}{\partial t}(\rho\overline{f'^2}) + \frac{\partial}{\partial x_i}(\rho u_i \overline{f'^2}) = -C_d\rho\frac{\varepsilon}{k}\overline{f'^2} + + \frac{\partial}{\partial x_i}\left(\frac{\mu_t}{\sigma_t}\frac{\partial}{\partial x_i}\overline{f'^2}\right) + C_g\mu_t\left(\frac{\partial}{\partial x_i}\bar{f}\right)^2$$

- Probability Density Function, p(f), let obtain local temperature from tabulated experimental results

$$\bar{T} = \int_0^1 p(f)T(f)df$$

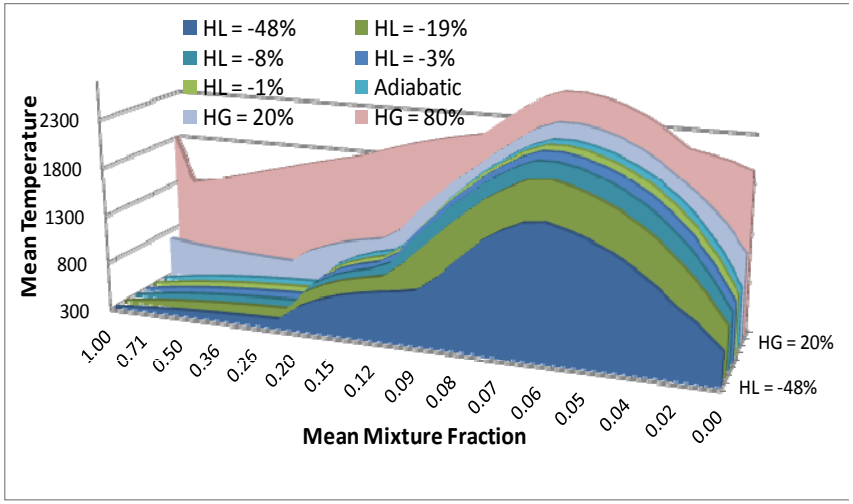

Influence of Swirl Number

- Contours of Mean Mixture Fractions are convex for mild swirling flows and concave for strong swirling case (90%CH_4)

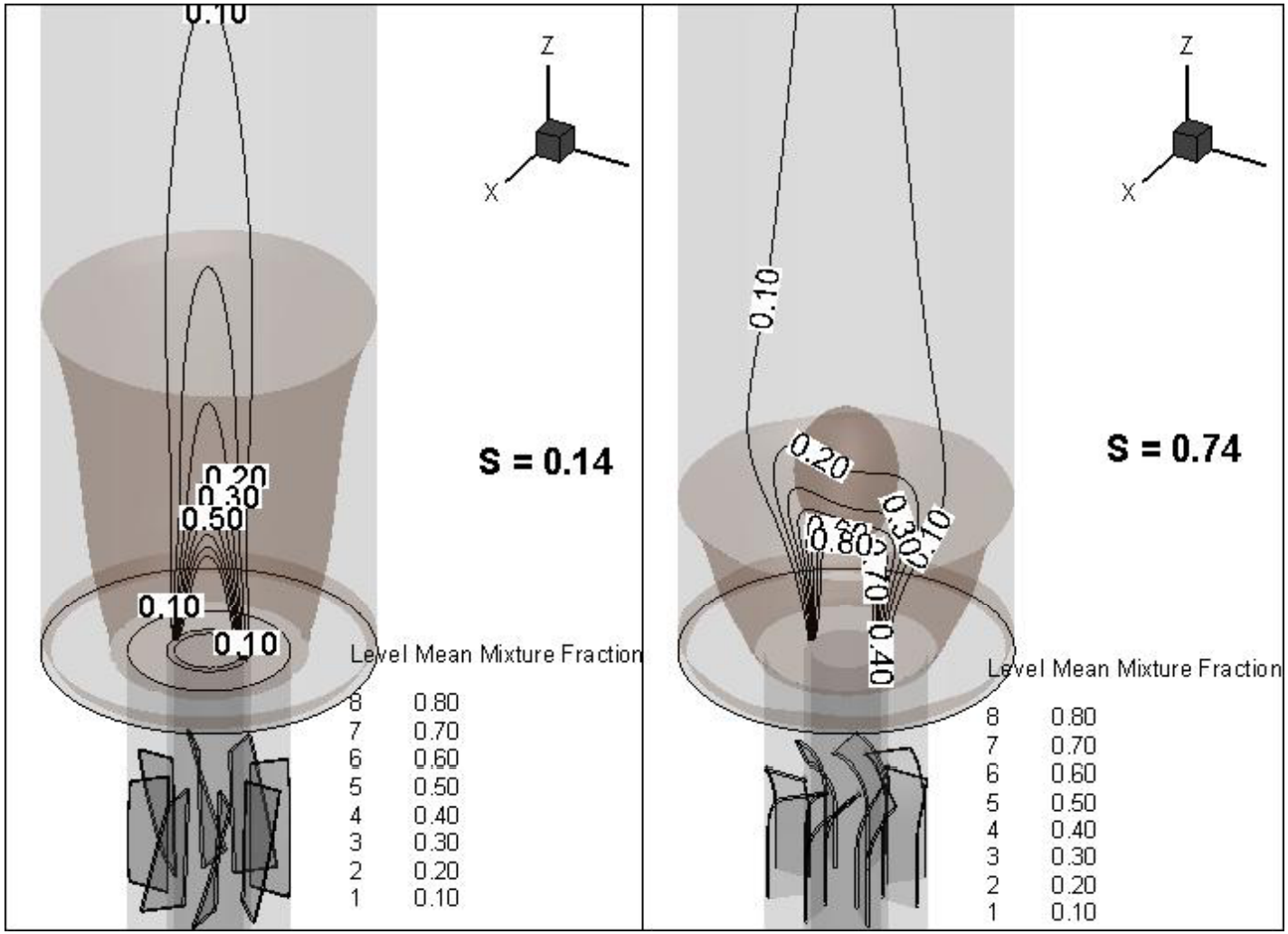

Contours of Mixture Fraction Variance for rich flame (90% CH4)

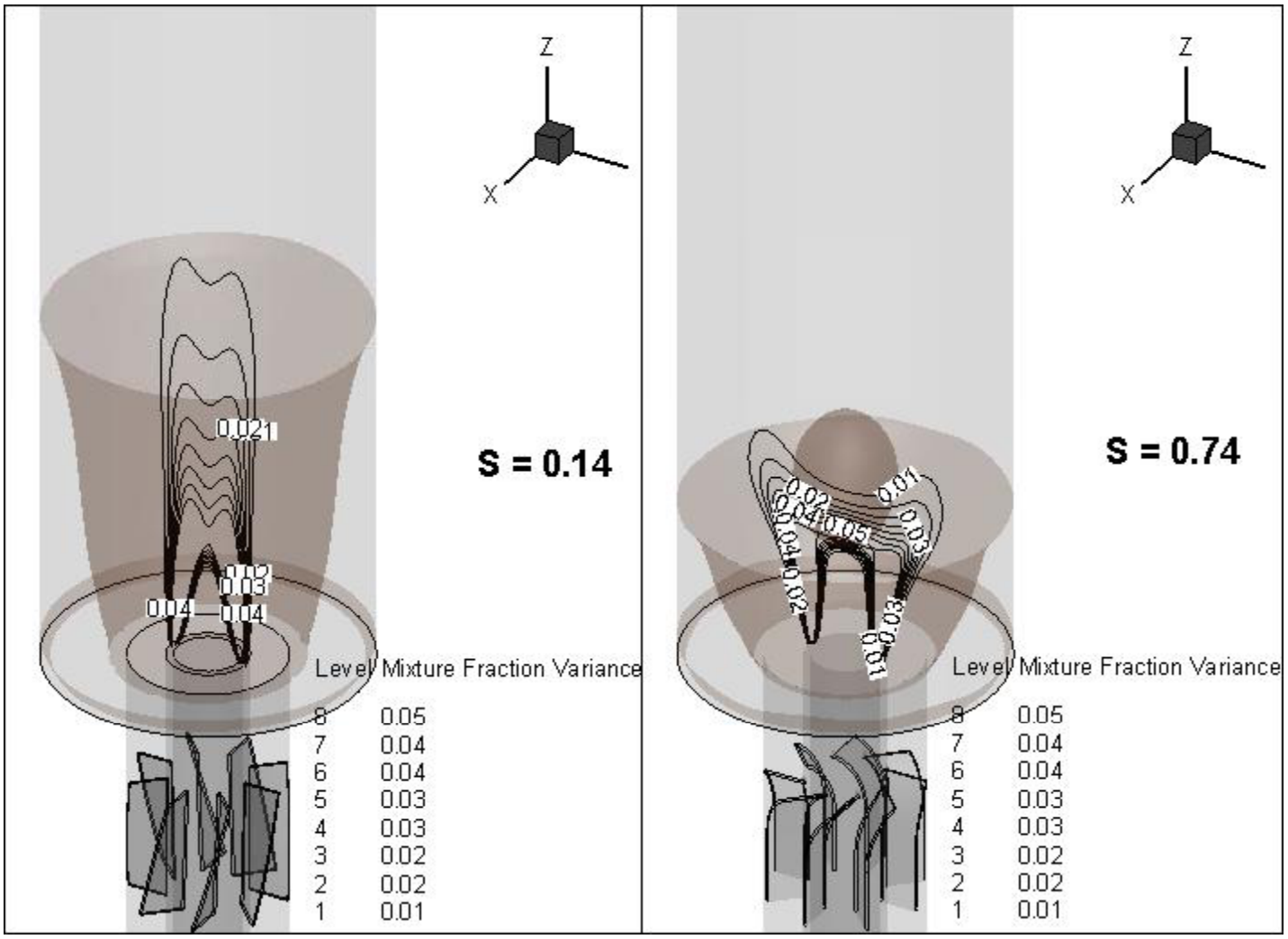

Contours of Temperature for rich flame (90% CH4)

- Bearing in mind the criterion to locate the flame front as the maximum temperature gradient, it is clear the thin reaction zone for swirl numbers of 0.74 and 0.95 located ahead of the lead stagnation point of the IRZ.
- In the case of swirl number 0.14, the lack of IRZ produces a thick reaction zone associate to weak temperature gradient.
- Numerical results predict no fuel reaches the IRZ even if other references assert it may be possible.

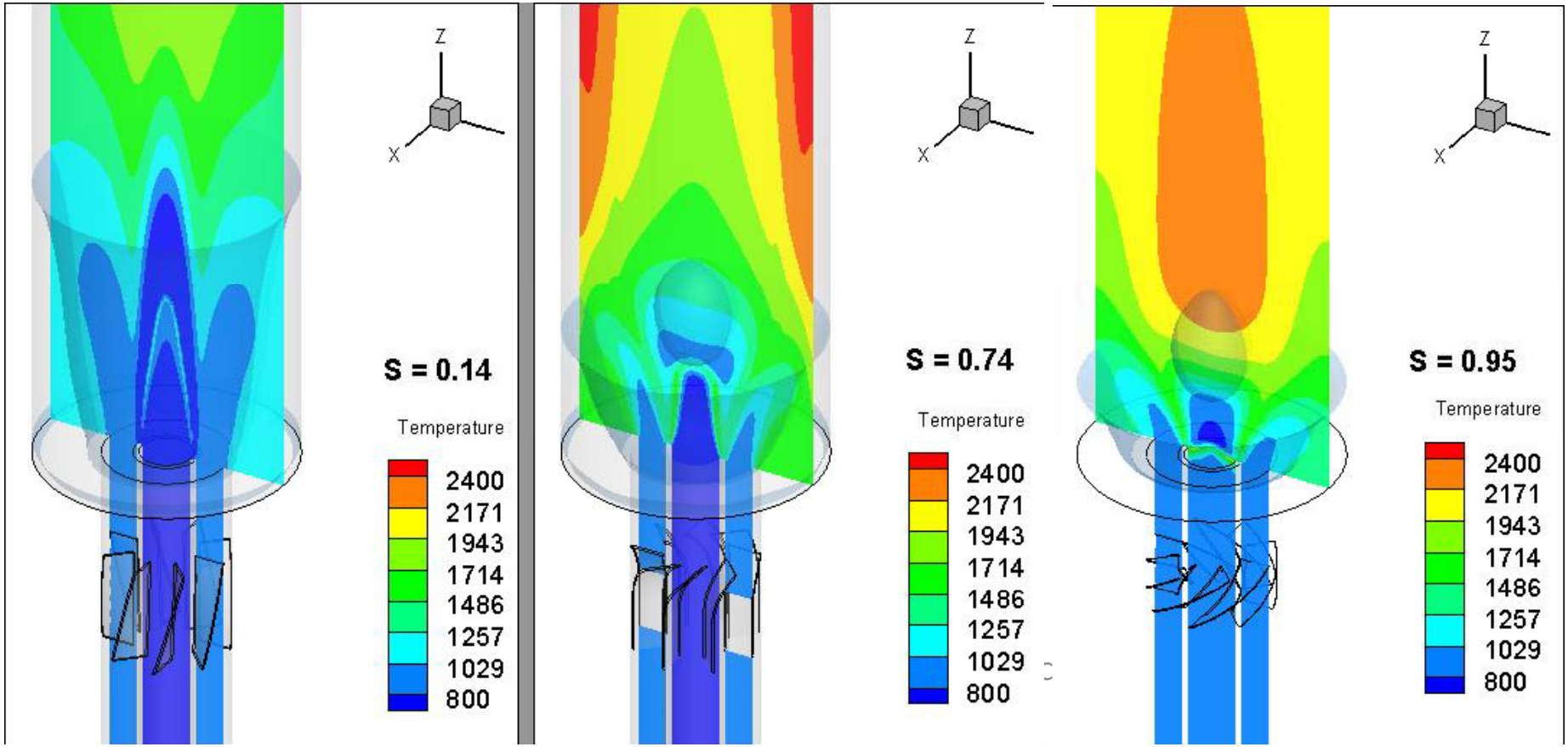

Radial profiles of Axial Velocity for reactive and non reactive cases

- Reactive cases (RXN) produce higher axial velocities than non reactive cases (noRXN) because there is a reduction of density in the reaction products
- It is clear the IRZ is higher for no reactive case than for the reactive one for swirl 0.74.

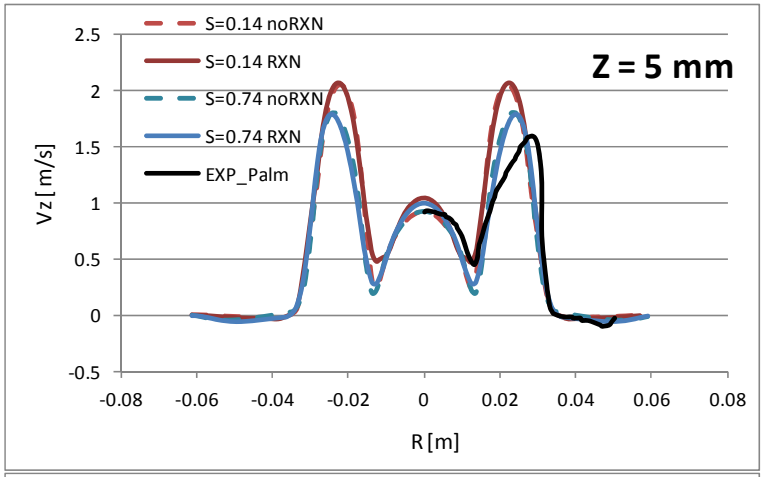

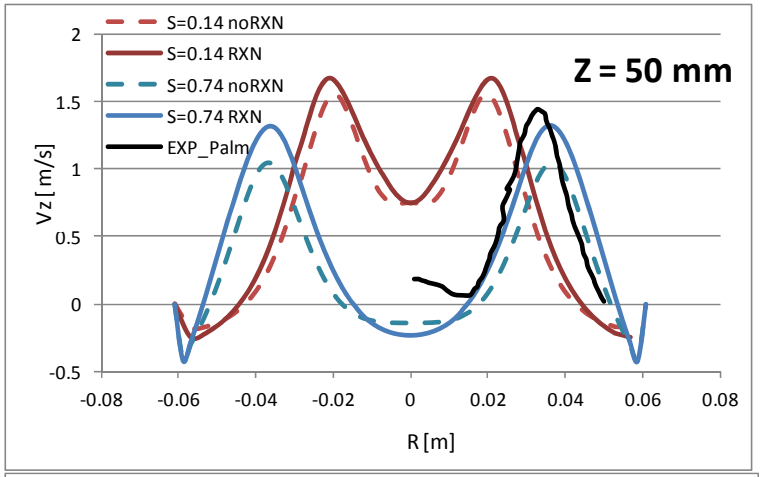

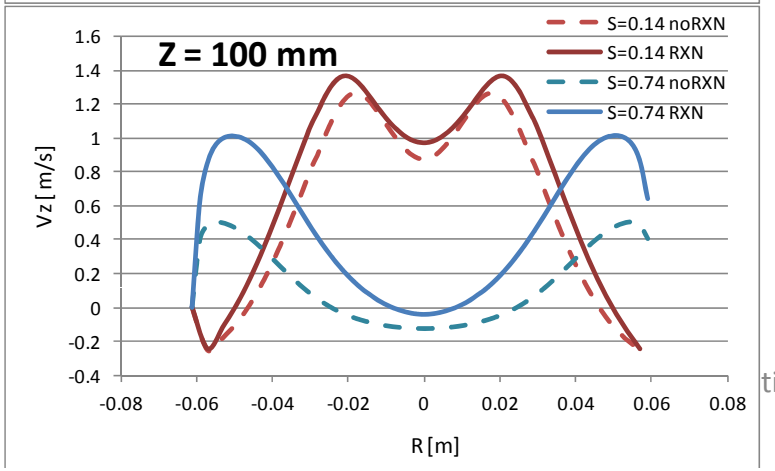

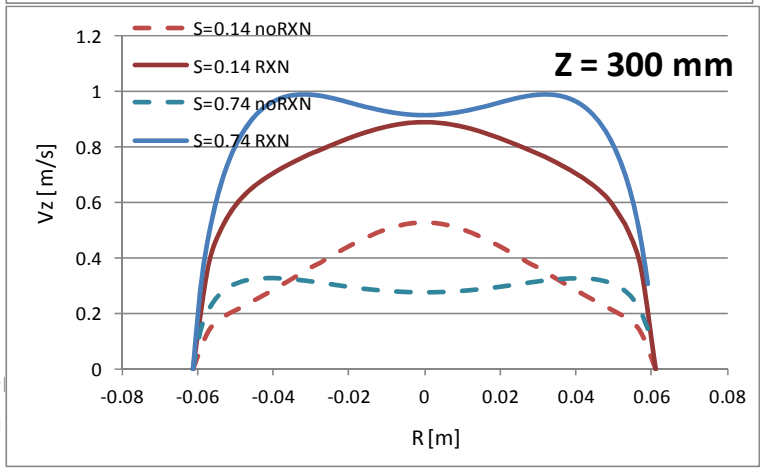

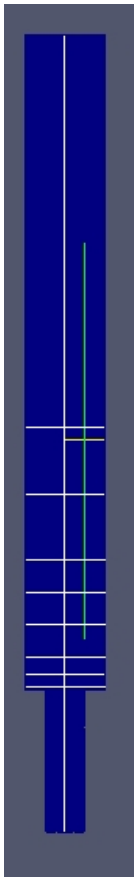

Radial profiles of Temperature for reactive and non reactive cases

- The maximum variance is observed for S=0.14, whereas for S=0.74 the flame is more compact in longitudinal direction

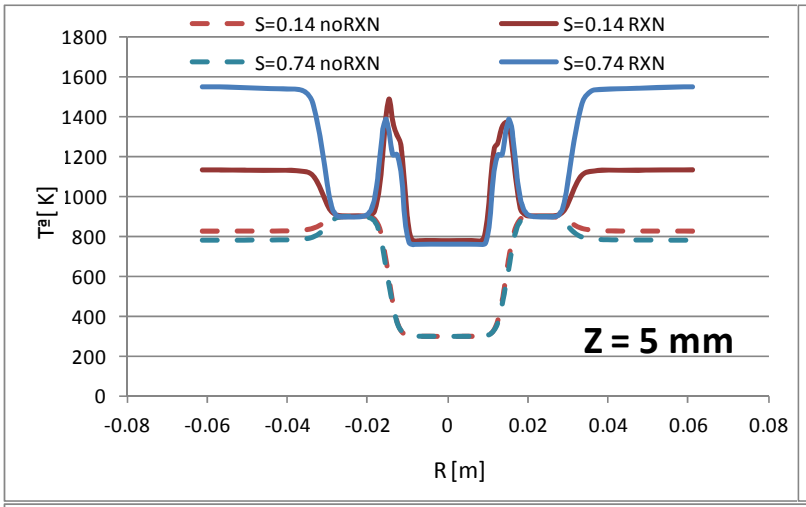

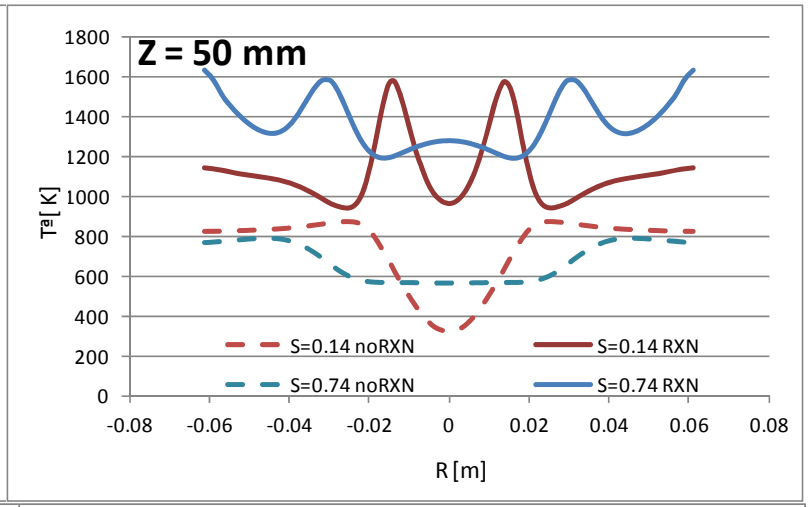

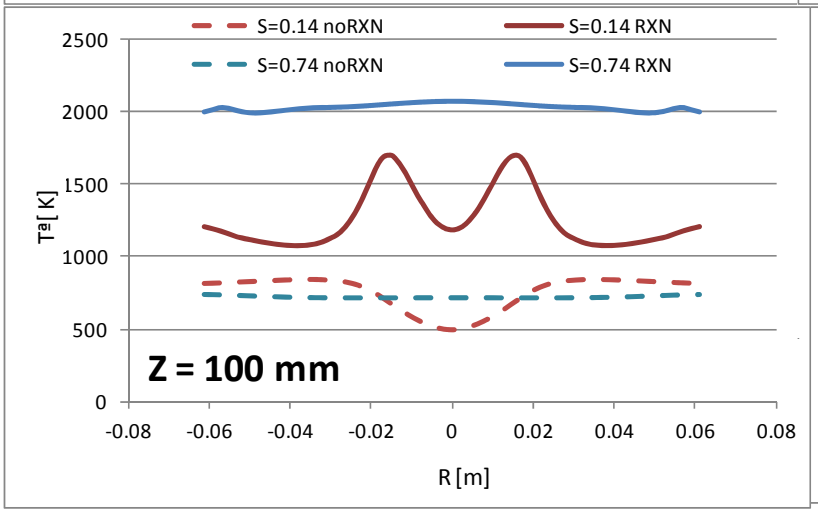

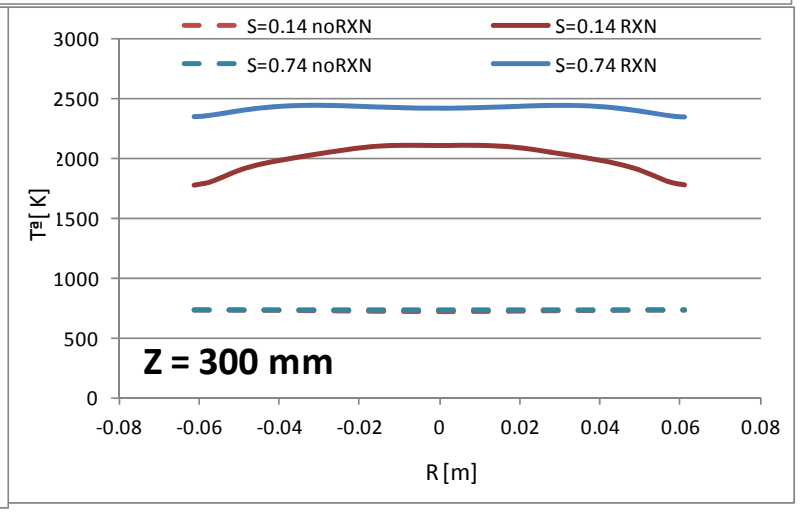

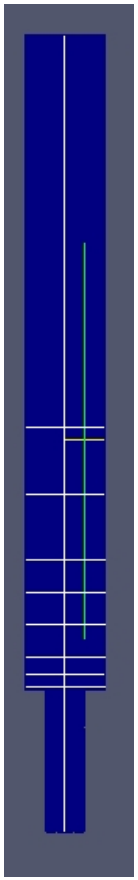

Influence of Stoichiometry

		Fuel	Air
Inlet		Central nozzle	Annular nozzle
Composition	**Stoichiometric mixture (λ=1)**	19% CH_4+81%N_2	22% O2, 78% N2
	Lean mixture (λ=1.2)	16% CH_4+84%N_2	
	Lean mixture (λ=1.4)	14% CH_4+86%N_2	
Temperature (K)		300	900
Velocity (m/s)		0.66	1.54
Turbulence Intensity (%)		12	7.5
Density (kg/m^3)		0.6679	1.225
Specific heat (J/kg/K)		Polynomial function of temperature	
Thermal conductivity (W/m/K)		0.0332	0.0242
Viscosity (kg/m/s)		1.087.10-5	1.7894.10-5
Molecular Weight (kg/kg/mol)			28.996

Contours of temperature for stoichiometric and lean flames

Swirl no. 0.14

Swirl no. 074

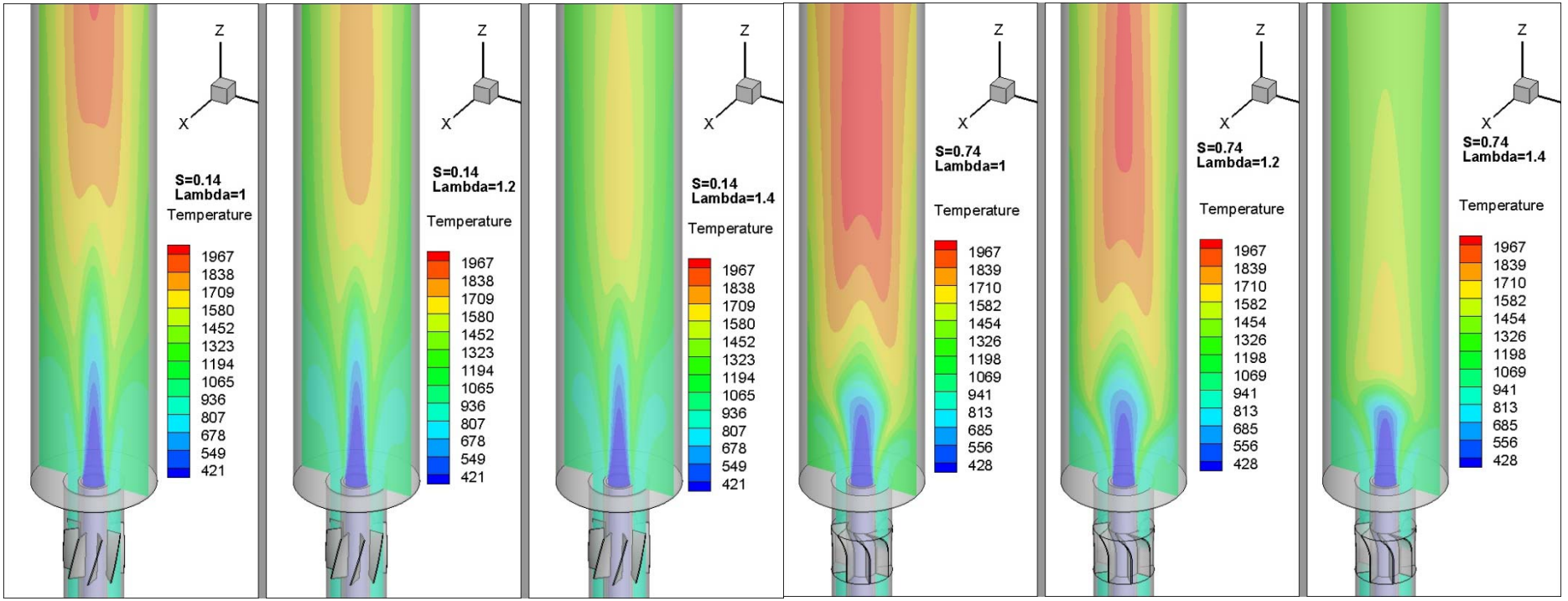

Contours of NO for stoichiometric and lean flames

Swirl no. 0.14

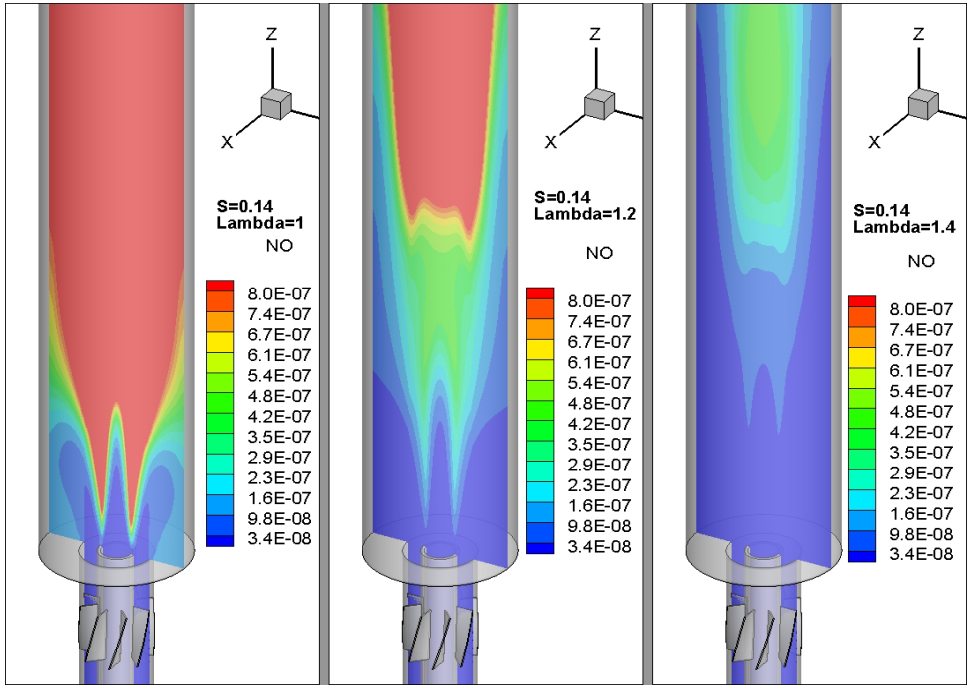

Swirl no. 074

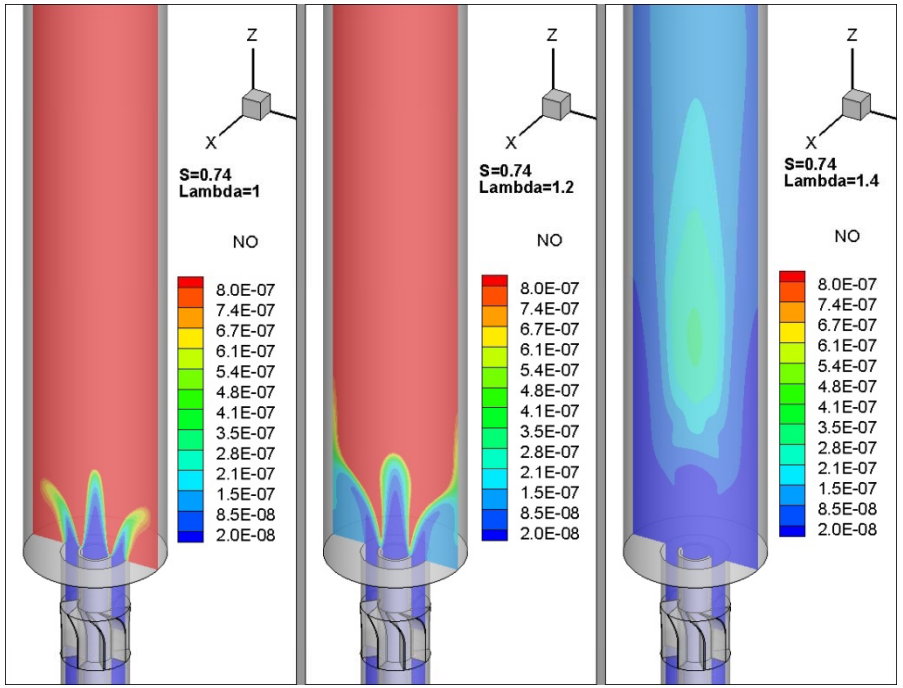

Conclusions of Reactive Cases

- Low swirling injectors do not promote the fluid to turn over near the centre of the chamber, resulting larger mixing and reaction zones with weak gradients of temperature and species' mass fractions.
- Whereas, high swirl burners promote the formation of an inner recirculation zone with hot products of reaction. The lead stagnation point of the IRZ plays an important role fixing the location of the flame front in swirling burners.
- At constant stoichiometry, the flame front is thinner and the equilibrium temperature as well as NO emissions are higher than those of low swirl burners.
- These aspects offer a chance of using lean mixtures with the corresponding reduction of methane consume and NO emissions.

Acknowledgements

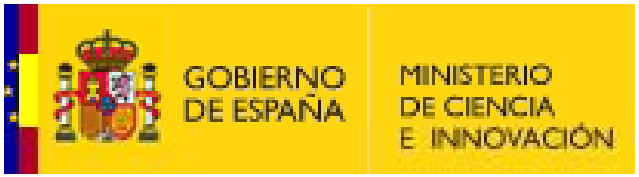

Ref. ENE2011-25468

HPC-Europa2
Pan-European Research Infrastructure on High Performance Computing

Grant no. 228398
application no. 1092

BSC Barcelona Supercomputing Center
Centro Nacional de Supercomputación

Ref. FI-2013-2-0002
and FI-2013-1-0001

PRACE

Ref. 2010PA1766

GENCI

DE LA RECHERCHE À L'INDUSTRIE
cea

Universidad de Valladolid

ESCUELA DE INGENIERÍAS INDUSTRIALES

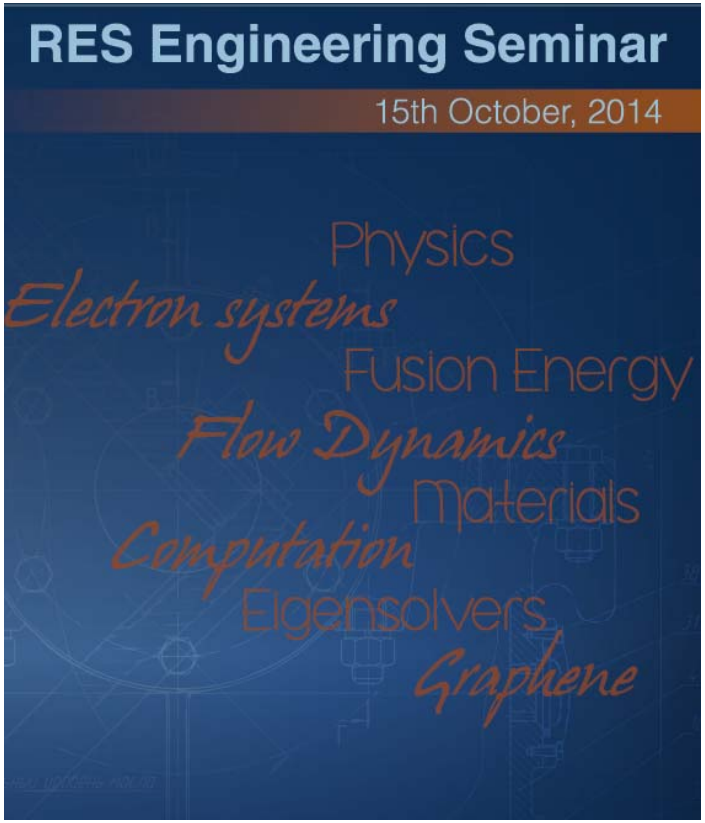

Thanks

terpar@eii.uva.es

Accepted Papers

[1] Parra-Santos M. Teresa, Mendoza-García Victor, Szasz Robert Z., Gutkowski Artur N., Castro-Ruiz Francisco "Influence of swirling on the aero-thermodynamic behaviour of flames" *Combustion Explosions and Shock Waves*.

Editorial: Springer Verlag ISSN: 0010-5082 Revised Version sent 30.03.14 ref. Manuscript 8141 Accepted 23.05.2014.

[2] Teresa Parra-Santos; Rubén J Pérez-Domínguez; Victor M Mendoza-García; Robert Z Szasz; Francisco Castro; Artur N Gutkowski; "An isothermal analysis of curved-vane and flat-vane swirlers for burners" *Engineering Computations*.

Editorial: Emerald ISSN: 0264-4401 Revised Version sent 29.03.14 ref. Manuscript ID EC-06-2013-0149.R1. Accepted 23.07.2014.

[3] Teresa Parra-Santos, Ville Vuorinen, Rubén Perez-Dominguez, Robert Szasz and Francisco Castro-Ruiz "Aerodynamic characterization of isothermal swirling flows in combustors" *International Journal of Energy and Environmental Engineering* 5:85 (2014) DOI 10.1007/s40095-014-0085-5

Editores: Springer Open ISSN 2008-9163

[4] T. Parra, R. Z. Szasz, C. Duwig, R. Pérez, V. Mendoza, and F. Castro "Acoustic Instabilities on Swirling Flames" *International Journal of Mechanical Engineering* Vol:7 No:9, 2013 pp 742-745

Editores: World Academy of Science, Engineering and Technology P-ISSN : 2010-376X International Science Index: http://www.waset.org/author/t-parra waset.org/publications/16734